

## **TITLE**

# **Trans-Synaptic Modulation of Kainate Receptor Functions by C1q-like Proteins**

## **AUTHORS**

Keiko Matsuda<sup>1,2,7</sup>, Timotheus Budisantoso<sup>1,2,7</sup>, Nikolaos Mitakidis<sup>3</sup>, Yuki Sugaya<sup>4</sup>,  
Eriko Miura<sup>1,2</sup>, Wataru Kakegawa<sup>1,2</sup>, Miwako Yamasaki<sup>2,5</sup>, Kotaro Konno<sup>2,5</sup>,  
Motokazu Uchigashima<sup>2,5</sup>, Manabu Abe<sup>2,6</sup>, Izumi Watanabe<sup>2,6</sup>, Masanobu Kano<sup>4</sup>,  
Masahiko Watanabe<sup>2,5</sup>, Kenji Sakimura<sup>2,6</sup>, A. Radu Aricescu<sup>3,8,\*</sup> & Michisuke Yuzaki<sup>1,2,8,\*</sup>

## **AFFILIATIONS**

<sup>1</sup>Department of Physiology, Keio University School of Medicine, Tokyo 160-8582, Japan.

<sup>2</sup>Core Research for Evolutional Science and Technology (CREST), Japan Science and Technology Agency (JST), Tokyo 102-0075, Japan.

<sup>3</sup>Division of Structural Biology, Wellcome Trust Centre for Human Genetics, University of Oxford, Oxford OX3 7BN, UK.

<sup>4</sup>Department of Neurophysiology, Graduate School of Medicine, University of Tokyo, Tokyo 113-0033, Japan.

<sup>5</sup>Department of Anatomy, Hokkaido University Graduate School of Medicine, Sapporo 060-8638 Japan.

<sup>6</sup>Department of Cellular Neurobiology, Brain Research Institute, Niigata University, Niigata 951-8585, Japan.

\*Correspondence: myuzaki@a5.keio.jp, radu@strubi.ox.ac.uk

---

<sup>7</sup>Co-first author. <sup>8</sup>Co-senior author.

## SUMMARY

Postsynaptic kainate-type glutamate receptors (KARs) regulate synaptic network activity through their slow channel kinetics, most prominently at mossy fiber (MF)–CA3 synapses in the hippocampus. Nevertheless, how KARs cluster and function at these synapses has been unclear. Here, we show that C1q-like proteins C1ql2 and C1ql3, produced by MFs, serve as extracellular organizers to recruit functional postsynaptic KAR complexes to the CA3 pyramidal neurons. C1ql2 and C1ql3 specifically bound the amino-terminal domains of postsynaptic GluK2 and GluK4 KAR subunits and the presynaptic neuexin 3 containing a specific sequence *in vitro*. In *C1ql2/3*-double null mice, CA3 synaptic responses lost the slow, KAR-mediated, components. Furthermore, despite induction of MF sprouting in a temporal lobe epilepsy model, KARs were not recruited to postsynaptic sites in *C1ql2/3*-double null mice, leading to reduced recurrent circuit activities. C1q-family proteins, broadly expressed, are likely to modulate KAR function throughout the brain and represent promising antiepileptic targets.

## INTRODUCTION

The vast majority of excitatory neurotransmission in the vertebrate brain is mediated by ionotropic glutamate receptors (iGluRs) comprised of four subfamilies: AMPA (GluA1–4), NMDA (GluN1–3), kainate (GluK1–5) and delta (GluD1–2). Different types of iGluRs are expressed at confined subcellular locations to achieve specific functions in neuronal circuits (Traynelis et al., 2010). While AMPA receptors mediate fast neurotransmission at the postsynaptic site, NMDA receptors regulate synaptic plasticity and cell survival at postsynaptic and extrasynaptic sites, respectively

(Hardingham and Bading, 2010). GluD2 is exclusively localized at the postsynaptic site of cerebellar Purkinje cells and gates long-term depression (LTD) of synaptic plasticity by regulating endocytosis of GluA2 AMPA receptors (Kohda et al., 2013). On the other hand, kainate receptors (KARs) have more diverse functions at both pre- and postsynaptic sites: KARs modulate neurotransmitter release at certain presynaptic sites, and regulate synaptic network activity through their slow channel kinetics at postsynaptic sites (Contractor et al., 2011; Lerma and Marques, 2013). Although recent high-resolution proteomics unraveled molecular diversity of native iGluR complexes (Schwenk et al., 2012; Shanks et al., 2012), it remains mostly unclear how certain iGluR subtypes are targeted to and function at specific subcellular sites.

Secreted C1q-family proteins, related to the C1q complement component (Kishore et al., 2004), have recently been identified as a new class of synapse organizers (Yuzaki, 2008). Cbln1, belonging to the cerebellin subfamily of C1q-like molecules, is released from cerebellar granule cells and plays a crucial role in the formation and function of parallel fiber–Purkinje cell synapses by binding to presynaptic neurexins containing a splice site 4 insert (Nrx+SS4) and the postsynaptic GluD2, to form a molecular triad that spans the synaptic cleft (Matsuda et al., 2010; Matsuda and Yuzaki, 2011; Uemura et al., 2010). Cbln1 not only regulates synapse formation, but also determines clustering of postsynaptic GluD2 by binding to its amino-terminal domain (ATD) (Matsuda et al., 2010). Similarly, neuronal pentraxins secreted from pre- and postsynaptic sites cause AMPA receptor clustering by mainly binding the ATD of GluA4 AMPA receptors in certain inhibitory neurons (Pelkey et al., 2015; Sia et al., 2007). These findings suggest that the ATD of iGluRs, the region most distal from the postsynaptic membrane, is used for interaction with transmembrane (Saglietti et al., 2007) and soluble proteins at the synaptic cleft to regulate the localization of iGluRs and/or their function at synapses. Nevertheless, synaptic proteins that

specifically interact with the ATD of KARs have not been identified so far.

KARs are highly enriched on the postsynaptic side of mossy fiber (MF)–pyramidal cell synapses in the hippocampal CA3 region and enhance synaptic integration during repetitive MF activities (Carta et al., 2014; Castillo et al., 1997). KARs are also enriched at postsynaptic sites of sprouted MFs in temporal lobe epilepsy and play a major role in the chronic seizures by enhancing the recurrent circuit activity (Peret et al., 2014). Intriguingly, mRNAs encoding the C1q-like (C1ql) subfamily C1ql2 and C1ql3 are highly expressed in dentate gyrus granule cells (DGCs) that send MFs (Iijima et al., 2010; Shimono et al., 2010). C1ql1, a C1ql subfamily member, was recently shown to be released from presynaptic sites and regulate maturation of synapses between climbing fibers and Purkinje cells by binding to brain angiogenesis inhibitor 3 (Bai3) in Purkinje cells (Kakegawa et al., 2015). Thus, we examined roles of C1ql2 and C1ql3 at MF–CA3 synapses. We demonstrate that C1ql2 and C1ql3 directly bind the ATD of postsynaptic GluK2 and GluK4 KARs, as well as a presynaptic Nr3 isoform that contains a specific sequence encoded by exon25b in splice site 5, which we refer to as Nr3+SS5<sup>25b</sup>. We found that the Nr3+SS5<sup>25b</sup>–C1ql2/3 complex is necessary and sufficient to recruit KARs at postsynaptic sites *in vitro*. In *C1ql2/3*-double null mice, no postsynaptic KARs were recruited to MF–CA3 synapses in control conditions, or to sprouted MFs in a temporal lobe epilepsy model, leading to reduced network activities. These results elucidate the physiological and pathological importance of the Nr3–C1ql2/3 signaling in regulating postsynaptic KAR functions.

## RESULTS

### **C1ql2 and C1ql3 proteins are localized at the MF–CA3 synaptic cleft**

We first investigated whether C1ql2 and C1ql3 proteins produced in DGCs (Iijima et al., 2010) can reach synaptic sites in the wild-type hippocampus, specifically the stratum lucidum in the CA3 region by specific antibody (Shimono et al., 2010). Immunohistochemical (IHC) analyses revealed that punctate C1ql2 (Shimono et al., 2010) and C1ql3 immunoreactivities were highly localized in the CA3 stratum lucidum of wild-type (Figures 1A and 1B). Using immunogold electron microscopy (EM), we confirmed that C1ql2 was mainly localized at the presynaptic MF terminals and their synaptic clefts (Figure 1C). Similarly, super-resolution fluorescence microscopy revealed that endogenous C1ql2 and C1ql3 were mainly localized between postsynaptic density 95 (PSD95)- and Bassoon-positive puncta in the CA3 stratum lucidum (Figure 1D). These findings indicate that C1ql2 and C1ql3 produced in the DGCs reach and localize at MF–CA3 synaptic clefts.

To investigate the physiological functions of C1ql2 and C1ql3, we generated mice in which the *C1ql2* and *C1ql3* genes were disrupted (Figure S1A–C). IHC (Figures 1A and 1B) and immunogold EM (Figure 1C) analyses revealed essentially no C1ql2 and C1ql3 immunoreactivities in *C1ql2*-null and *C1ql3*-null hippocampus, respectively. Unexpectedly, gross anatomy of the hippocampus (Figure S1D) and MF projection patterns (Figure S1E) were unaffected in these mice. Similarly, the distribution of vesicular glutamate transporter 1 (vGluT1)-immunopositive MF terminals (Figure S1F), as well as PSD95 immunoreactivities (Figure S1G), were unaffected in *C1ql2*- or *C1ql3*-null CA3 stratum lucidum. To exclude potential functional redundancy and/or compensation between C1ql2 and C1ql3, we generated *C1ql2/3*-double null mice (Figure S1C). *C1ql2* and *C1ql3* double heterozygous breeding pairs (*C1ql2*<sup>+/-</sup>; *C1ql3*<sup>+/-</sup>) produced the expected frequencies of double homozygous null offspring (6%). *C1ql2/3* double-null mice were fertile and produced offspring with normal sex ratios (52%

female). No differences in body weights were observed between wild-type and *C1ql2/3*-null mice at birth (WT,  $1.33 \pm 0.03$  g,  $n = 31$ ; *C1ql2/3*-null,  $1.30 \pm 0.02$  g,  $n = 40$ ;  $p > 0.05$ ) and at postnatal 4 weeks (male WT,  $12.6 \pm 0.4$  g,  $n = 13$ ; male *C1ql2/3*-null,  $12.7 \pm 0.5$  g,  $n = 12$ ,  $p > 0.05$ ; female WT,  $11.8 \pm 0.3$  g,  $n = 18$ ; male *C1ql2/3*-null,  $11.7 \pm 0.4$  g,  $n = 19$ ,  $p > 0.05$ ). Gross anatomy of the hippocampus (Figures S1D), MF projection patterns (Figure S1E), the distribution of vGluT1 (Figure S1F) and PSD95 immunoreactivities (Figure S1G) were also unaffected in *C1ql2/3* double-null mice. These results suggest that, unlike other C1q-family proteins, such as Cbln1 (Matsuda et al., 2010; Uemura et al., 2010) and C1ql1 (Kakegawa et al., 2015), C1ql2/3 do not regulate synapse formation *per se* in the hippocampus.

### **The ATDs of GluK2/4 serve as postsynaptic receptors for C1ql2/3 *in vitro* and *in vivo***

Localization of C1ql2 and C1ql3 immunoreactivities closely matched that of GluK2/3 KAR in the CA3 stratum lucidum (Figure 1A). Since GluD1 and GluD2 serve as postsynaptic receptors for Cbln1 through their ATDs (Matsuda et al., 2010), we hypothesized that ATDs of KARs may be associated with C1q-like proteins. To test this hypothesis, we first performed cell-based binding assays by expressing the ATD of various iGluRs on the surface of HEK293 cells and applying HA-tagged recombinant full-length C1ql2 and C1ql3 (Figure 2A). Interestingly, C1ql2 and C1ql3 specifically bound to cells expressing the AMPA receptor subunit GluA1 as well as the KAR subunits GluK2 and GluK4, respectively (Figures 2A and 2B). C1ql2 and C1ql3 did not show any binding to the ATDs of other AMPA, kainate, NMDA or delta receptor subunits (Figures 2A and 2B). To further investigate the interaction specificity between C1ql2/3 and GluK ATDs, we created various chimeric proteins between the ATDs of GluK2 and GluK3 because, despite the sequence similarity of their ATDs (Figure S3A), C1ql2/3 specifically bound to GluK2

(Figures 2A and 2B). Cell-based binding assays (Figure S3B) revealed that L3 and L4 regions, but not L1 and L2 regions, of GluK2 were required for binding to C1ql3 (Figure S3C). In addition, C1ql3 binding to GluK2-ATD was significantly reduced when 3 amino acid residues in the L3 region (K306–D308) or 9 residues in the L4 region (V329–F337) were substituted with the corresponding residues of GluK3-ATD (Figure S3C). However, similar motifs were not found in the corresponding regions of the ATDs of GluA1 and GluK4. Thus, to completely understand how C1ql2/3 specifically bind to the ATDs of GluA1/GluK2/4, structures of protein complexes will need to be solved in future studies.

To test whether C1ql2 and C1ql3 associate with these receptors *in vivo*, we next examined *GluK2*-null (Figures S2A–C) and *GluK4*-null (Akashi et al., 2009) hippocampi. IHC analyses revealed that C1ql2 (Figure 2C) and C1ql3 (Figure 2D) immunoreactivities were significantly reduced in the CA3 stratum lucidum of *GluK2*-null and *GluK4*-null hippocampi. Remaining C1ql2 (Figure 2C) and C1ql3 (Figure 2D) immunoreactivities were significantly lower in *GluK2*-null than in *GluK4*-null hippocampal tissues. This may reflect loss of both GluK2 and GluK4 from the surface of *GluK2*-null neurons because GluK4 absolutely depends on GluK2 for cell surface trafficking (Pahl et al., 2014). In contrast, C1ql2 immunoreactivity was unaffected in the hippocampal CA3 regions in *GluA1*-null mouse (Figure S2D). In addition, unlike GluK2/3 immunoreactivity in the CA3 stratum lucidum (Figures 1A and S2C), GluA1 immunoreactivity was also observed in the stratum radiatum (Figure S2E). These results indicate that although GluA1 may play roles in other synapses, it does not serve as an endogenous receptor for C1ql2 and C1ql3 at MF–CA3 synapses.

GluK2 is highly expressed at postsynaptic sites, but functional KARs are also reported at presynaptic sites of MF–CA3 synapses (Contractor et al., 2000; Kamiya and Ozawa, 2000; Lerma

and Marques, 2013). Thus, to clarify the contribution by the postsynaptic GluK2, we next knocked out the gene encoding GluK2 in CA3 pyramidal neurons by crossing GluK4-*Cre* driver mice (*GluK4<sup>Cre/+</sup>*), which predominantly induced recombination in CA3 pyramidal neurons (Akashi et al., 2009), with *GluK2<sup>flox/flox</sup>* mice. IHC analyses revealed that C1ql2 immunoreactivity in the CA3 stratum lucidum in *GluK2<sup>flox/flox</sup>*; *GluK4<sup>Cre/+</sup>* mice was reduced to the level similar to that in *GluK2*-null mice (Figure S2F), suggesting that postsynaptic GluK2 was mainly responsible for C1ql2 localization at these synapses. Finally, we used surface plasmon resonance to measure the interactions between the trimeric gC1q domains of C1ql2 and C1ql3 and the dimeric GluK2 ATD (Figure 2E), and found these to be in the low micro-molar range (5.6  $\mu$ M and 3.38  $\mu$ M, respectively; Figure 2F). None of the gC1q constructs bound to the ATDs of GluK3 or GluK5 (Figures 2F, S3D and S3E).

Taken together, these results indicate that GluK2 and GluK4 serve as endogenous receptors for C1ql2 and C1ql3 at the MF–CA3 synapses in the hippocampus *in vivo* and that the ATDs of GluK2 and GluK4 directly and specifically bind the globular domains of C1ql2 and C1ql3.

### **C1ql2 and C1ql3: master regulators of postsynaptic KAR complexes**

What functions do C1ql2/3 play at MF–CA3 synapses? Interestingly, IHC analyses revealed that although synaptic GluK2/3 immunoreactivity in the CA3 stratum lucidum was unaffected in single *C1ql2*-null or *C1ql3*-null mice (Figure S1H), it markedly decreased in double null (*C1ql2/3*-null) mice (Figures 3A and S1H). In contrast, no changes were observed for GluA1 immunoreactivity in *C1ql2/3*-null mice (Figure S2E), a result consistent with the view that GluA1 does not associate with endogenous C1ql2 in the CA3 stratum lucidum (Figure S2D). Immunogold EM analysis further confirmed loss of GluK2/3 immunoreactivity, which was mainly

observed at the postsynaptic site in wild-type CA3 pyramidal neurons (Petrálie et al., 1994), in both *C1ql2/3*-null and *GluK2*-null mice, despite the absence of changes in PSD lengths (Figure 3B). In contrast, immunoblot analysis showed that total GluK2/3 protein levels were similar in the CA3 stratum lucidum regions between wild-type and *C1ql2/3*-null mice (Figure 3C). In addition, extrasynaptic GluK2/3 immunoreactivity was clearly present in the CA3 region of *C1ql2/3*-null mice (Figure S2C). These results indicate that postsynaptic localization, but not the amount of KARs, was regulated by C1ql2 and C1ql3 in CA3 pyramidal neurons.

Neuropilin and tolloid-like 1 (Neto1), an auxiliary KAR subunit that determines the slow EPSC kinetics, is specifically expressed on the postsynaptic side of at MF–CA3 synapses (Copits and Swanson, 2012; Straub et al., 2011). However, it remains unclear whether Neto1 is involved in postsynaptic trafficking of KARs in CA3 pyramidal cells (Pahl et al., 2014), and how Neto1 itself is targeted to the postsynaptic site (Pahl et al., 2014; Straub et al., 2011; Tang et al., 2011). IHC analyses revealed that Neto1 immunoreactivity decreased significantly in the CA3 stratum lucidum of *C1ql2/3*-double null mice, but not in single *C1ql2*-null or *C1ql3*-null mice (Figure 3D). Unlike KARs, the extracellular domains of Neto proteins did not show any binding to recombinant C1ql2 or C1ql3 in cell-based binding assays (Figure 2B, middle). Similarly, immunoreactivities of GluK4 and GluK5, KAR subunits that require GluK1–3 for surface expression and determine the high affinities for kainate, were significantly reduced in the CA3 stratum lucidum to the levels observed in *GluK2*-null mice (Figure 3E). These results indicate that C1ql2 and C1ql3 likely regulate postsynaptic localization of Neto1 and GluK5 indirectly, by binding to GluK2/4, and that C1ql2 and C1ql3 serve as anterograde master regulators for postsynaptic localization and function of KAR complexes in CA3 pyramidal neurons.

To clarify whether C1ql2 or C1ql3 alone could regulate localization of KARs *in vivo*, we

next examined synapses formed on DGCs by hilar mossy cells, which expressed only C1ql3, but not C1ql2 mRNA (Figure S4A). IHC analyses revealed that GluK2 and GluK5 immunoreactivities (Figures S4B and S4C) were severely reduced at the mossy cell–DGC synapses in the inner molecular layer of *C1ql3*-null, but not in *C1ql2*-null dentate gyrus, indicating that C1ql3 alone was sufficient to recruit postsynaptic KARs on DGCs *in vivo*. These data suggest that the reason why localization of postsynaptic KAR complexes were unaffected in single *C1ql2*- or *C1ql3*-null MF–CA3 synapses (Figures 3D and S1H) was because either C1ql2 or C1ql3 alone could recruit KAR complexes to these synapses.

In addition to the hippocampus, KARs are expressed in various brain regions, including the cerebellum and the striatum (Figures S4D and S4E). Immunoblot analyses revealed expression of C1ql3, but not C1ql2, in the striatum, and absence of C1ql2 and C1ql3 in the cerebellum (Figure S4F). Consistent with these findings, KAR immunoreactivity was similar between wild-type and *C1ql2/3*-null cerebellum (Figure S4D). By contrast, we found that synaptic KARs disappeared in *C1ql2/3*-null, as well as in *GluK2*-null striatum (Figure S4E). Since C1ql2/3 mRNA signals are absent in the striatum (Iijima et al., 2010), these results indicate that like C1ql2/3 provided by mossy fibers, C1ql3 derived from projecting fibers to the striatum, such as corticostriatal inputs, may regulate synaptic localization of KARs in the striatum. Together, although there may be other mechanisms by which KARs trafficking is controlled, C1ql2/3 likely regulate synaptic localization and function of KARs in multiple brain regions.

Bai3, a cell-adhesion G protein-coupled receptor, was previously shown to serve as a receptor for C1q-like proteins C1ql1–4 *in vitro* and *in vivo* (Bolliger et al., 2011; Kakegawa et al., 2015). To explore the possibility that Bai3, or its closely related member Bai2 (Kakegawa et al., 2015), play a similar role at MF–CA3 synapses, we examined double *Bai2/3*-null mice. Although C1ql1

immunoreactivity was completely lost in the *Bai3*-null cerebellum (Kakegawa et al., 2015), C1ql2 and C1ql3 immunoreactivities were unaffected at MF–CA3 synapses in double *Bai2/3*-null mice (Figures S5A and S5B). Similarly, no changes were observed for GluK2/3 immunoreactivity in the CA3 stratum lucidum of *Bai2/3*-null mice (Figure S5C). Interestingly, IHC analysis revealed that Bai3 immunoreactivity was very low in the CA3 stratum lucidum (Figure S5D). These results indicate that Bai3 is unlikely involved in C1ql2/3–KAR signaling at MF–CA3 synapses, and that C1ql proteins may play distinct roles depending on their postsynaptic receptor type.

### **C1ql2/3 directly bind to Nr3 containing the SS5<sup>25b</sup> insert**

A unique feature of the secreted synaptic organizer Cbln1 is that it functions as a connector between pre- and postsynaptic receptors, Nr3+SS4 and GluD2, respectively (Matsuda et al., 2010; Uemura et al., 2010). To explore the possibility that C1ql2 and C1ql3 may also interact with neurexins, we performed cell-based binding assays by expressing various major Nr3 isoforms in HEK293 cells (Figure 4A). We found that full-length C1ql2 and C1ql3 specifically bound HEK293 cells expressing Nr3 $\beta$  (Figure 4B). While the SS4 insert was essential for Cbln1 to bind to all Nr3 isoforms, the presence or absence of SS4 in Nr3 $\alpha$ , Nr3 $\beta$ , Nr3 $\gamma$  and Nr3 $\delta$  did not affect their binding to C1ql2 or C1ql3 (Figure 4B). Another alternative splicing at site 5 (SS5) is reported to produce an isoform unique to Nr3 that contains a sequence encoded by exon 25b (SS5<sup>25b</sup>) in approximately half of Nr3 $\beta$  transcripts (Schreiner et al., 2014; Treutlein et al., 2014). Thus, we next examined the effect of the SS5<sup>25b</sup> sequence. Interestingly, Nr3 $\beta$  lacking SS5<sup>25b</sup> significantly lost binding ability to C1ql2 and C1ql3 (Figure 4B). Although certain Nr2 isoforms contain an equivalent sequence encoded by exon 23 at SS5 (Figures 4A and S6A), the presence of this sequence did not affect its binding to C1ql3 (Figures 4C and 4D).

Nrx3 $\beta$  also contains a  $\beta$ -specific region encoded by exon 18 (Figure 4A) in addition to common exons 19–25 shared with Nrx3 $\alpha$ . However, we found that C1ql3 bound Nrx3 $\beta$  lacking this  $\beta$ -specific sequence (Figures 4C and 4D). Indeed, C1ql3 bound Nrx3 $\alpha$  lacking the  $\beta$ -specific sequence but containing SS5<sup>25b</sup> (Figure S6B). These results indicate that the SS5<sup>25b</sup> sequence, encoded by exon25b of Nrx3, provides a binding site for C1ql2 and C1ql3.

To further define the determinants of interaction between C1ql2/3 and the ectodomain of Nrx3 $\beta$  with (ect-Nrx3 $\beta$ +SS5<sup>25b</sup>) or without (ect-Nrx3 $\beta$ -SS5<sup>25b</sup>) the SS5<sup>25b</sup> sequence, we used surface plasmon resonance assays (Figure 4E). We found that the ectodomain of Nrx3 $\beta$ +SS5<sup>25b</sup>, but not that of Nrx3 $\beta$ -SS5<sup>25b</sup>, bound the gC1q domains of C1ql2 and C1ql3 in the low micro-molar range (14.9  $\mu$ M and 8.6  $\mu$ M, respectively; Figures 4F and S6C). Subsequently, we narrowed down the minimal binding site within the region encoded by Nrx3 exon 25b and found that a sequence consisting of 17 amino acids, which we refer to as S5-9 (Figure S6A), bound C1ql3 (Figure S6D). Surface plasmon resonance measurements revealed that the gC1q domain of C1ql3 bound the isolated S5-9 peptide with an affinity comparable to full length ect-Nrx3 $\beta$ +SS5<sup>25b</sup> ( $K_D$  = 4.7  $\mu$ M, Figures 4G and S6E). Although full length C1ql2 and C1ql3 weakly bound Nrx3 that does not contain the SS5<sup>25b</sup> sequence (Figures 4C, 4D, 4H and S6C), these results demonstrate that exon 25b of Nrx3 is used as a specific splicing determinant for its association with C1ql2 and C1ql3.

### **The Nrx3-C1ql2/3 complexes serve as synaptic partners for KARs *in vitro***

To define the roles for Nrx3–C1ql2/3 interactions in organizing KAR-containing synapses, we expressed Nrx3 $\beta$ +SS5<sup>25b</sup> together with C1ql2 and C1ql3 (C1ql2+3) on the surface of HEK293 cells and co-cultured them with *C1ql2/3*-null hippocampal neurons. We found that endogenous GluK2/3, as well as neuroligin 1 (NL1, a receptor that binds to all Nrx isoforms) and PSD95,

accumulated in hippocampal neurons contacting HEK293 cells (Figure 5A). However, when Nr $\alpha$ 3 $\beta$ +SS5<sup>25b</sup> was expressed without C1ql2+3, NL1 and PSD95, but not GluK2/3, formed clusters in *C1ql2/3*-null hippocampal neurons (Figure 5A). Conversely, when Nr $\alpha$ 3 $\beta$ +SS5<sup>25b</sup> lacking the laminin/neurexin/sex hormone-binding globulin (LNS) domain, which is necessary and sufficient for its binding to NL1 (Gokce and Sudhof, 2013), was co-expressed with C1ql2+3 in HEK293 cells, only GluK2/3 were recruited in the contacted hippocampal neurons (Figure 5B). These data suggest that Nr $\alpha$ 3 $\beta$ +SS5<sup>25b</sup> may participate in hemi-synapse formation by using two distinct domains, the LNS domain and the SS5<sup>25b</sup> sequence, for NL1 and C1ql2/3 interactions, respectively. Co-expression of Nr $\alpha$ 3 $\beta$ +SS5<sup>25b</sup> together with either C1ql2 or C1ql3 alone in HEK293 cells also caused accumulation of GluK2/3 in *C1ql2/3*-null hippocampal neurons (Figure 5C), indicating that the Nr $\alpha$ 3–C1ql2/3 complex could function as a presynaptic partner for postsynaptic KARs *in vitro*.

To further define the role of the Nr $\alpha$ 3–C1ql2/3 complex components in synapse organization, we used a bead-induced synaptic differentiation assay (Matsuda et al., 2010). When beads coated with C1ql3 (Figure 5D) were co-cultured with *C1ql2/3*-null hippocampal neurons, endogenous GluK2/3 receptors were recruited around the beads. These data indicate that, besides other potential roles, Nr $\alpha$ 3 serves as a scaffold to accumulate C1ql2/3 for recruiting postsynaptic KARs.

### **C1ql2/3 regulate postsynaptic functions of KAR at MF–CA3 synapses *in vivo*.**

To define the functional roles of C1ql2/3 in MF–CA3 synaptic transmission, we next performed whole-cell patch-clamp recordings from CA3 pyramidal neurons in *C1ql2/3*-null hippocampal slices. KAR-mediated EPSC components were evaluated in the presence of 60  $\mu$ M GYKI52466, a

selective AMPAR antagonist. MF-evoked ESPCs were reduced to approximately 15 % (Figure 6A). MF-EPSCs were more strongly inhibited by GYKI52466 in *GluK2*-null mice (Figure 6A, top traces and graph) and the remaining MF-EPSCs did not show slow decay (Figure 6A, bottom traces and graph), indicating that slow EPSC components in wild-type mice were mostly mediated by KARs (EPSC<sub>KAR</sub>), which could be isolated by GYKI53655. Importantly, the amplitude (Figure 6A, top traces and graph) and the decay time constant (Figure 6A, bottom traces and graph) of MF-evoked EPSCs were reduced in *C1ql2/3*-null mice to levels similar to those of *GluK2*-null mice. The slow decay contributed to EPSC<sub>KAR</sub> summation when MFs were stimulated at high frequency in wild-type, but not in *C1ql2/3*-null, hippocampal slices (Figure 6B). Similarly, the likelihood of action potential initiation during repetitive MF stimulation was significantly lower in *C1ql2/3*-null CA3 pyramidal neurons (Figure 6C). In contrast, the amplitude and kinetics of AMPAR-mediated quantal EPSCs elicited by MF stimulation in the presence of Sr<sup>2+</sup> was similar between wild-type and *C1ql2/3*-null CA3 neurons (Figure 6D). Similarly, the ratios between NMDAR and AMPAR components of MF-EPSCs in wild-type and *C1ql2/3*-null CA3 pyramidal neurons were comparable (Figure 6E). These results indicate that postsynaptic KARs, but not AMPARs or NMDARs, were selectively regulated by *C1ql2/3* and enhanced synaptic integration during repetitive MF activities.

*GluK2* and *GluK5* are also thought to be expressed at the presynaptic site of MFs and to regulate glutamate release (Contractor et al., 2000; Kamiya and Ozawa, 2000; Lerma and Marques, 2013). To examine whether the functions of presynaptic KARs were regulated by *C1ql2/3* and contribute to the frequency facilitation, we tested the effect of low concentrations of kainate on MF-EPSCs. In wild-type and *C1ql2/3*-null, but not in *GluK2*-null hippocampus, MF-EPSCs were significantly reduced by 3  $\mu$ M kainate (Figure 6F), reflecting the function of presynaptic KARs.

Similarly, although the paired-pulse facilitation ratios (PPR) of EPSCs, which reflects glutamate release probability, were similar in wild-type, *C1ql2/3*-null and *GluK2*-null CA3 synapse at 50-ms intervals, treatment with 3  $\mu$ M KA failed to increase the PPR in *GluK2*-null (Contractor et al., 2000), but not in wild-type and *C1ql2/3*-null CA3 synapses (Figure 6F). These results are consistent with those obtained from IHC and EM analyses, further indicating that *C1ql2/3* do not affect the function of presynaptic KARs at MF–CA3 synapses.

### ***C1ql2/3* recruit postsynaptic KARs at sprouted MFs in a chronic epilepsy model.**

In human temporal lobe epilepsy, sprouting of hippocampal MFs and accumulation of associated KARs leads to the formation of pathological recurrent excitatory circuits in the DGCs (Lerma and Marques, 2013; Peret et al., 2014). To examine how *C1ql2/3* contribute to this pathological condition, we used an *in vitro* epilepsy model, in which organotypic hippocampal slice cultures were treated with pilocarpine (Peret et al., 2014). Six days after the treatment, IHC analyses of the dentate gyrus revealed similar levels of sprouted MFs in wild-type and *C1ql2/3*-null mice (Figure 7A) (Grabs et al., 1994; Peret et al., 2014). Whole-cell recordings from pilocarpine-treated DGCs (Figure 7B) showed slowly decaying spontaneous EPSCs (the time constant,  $6.1 \pm 0.2$  ms,  $n = 19$ ), which was quite similar to the one ( $\sim 6.2$  ms) previously reported in DGCs in pilocarpine-treated organotypic hippocampal slices in the presence of GYKI53655, another selective AMPAR antagonist (Peret et al., 2014). These results indicate that postsynaptic KARs were recruited to wild-type DGCs. In contrast, essentially no slow spontaneous EPSCs were recorded in pilocarpine-treated *C1ql2/3*-null DGCs in the presence or absence of GYKI52466 (Figure 7B), as reported for pilocarpine-treated *GluK2*-null DGCs (Peret et al., 2014). Extracellular field recordings also revealed stereotyped spontaneous interictal-like activity consisting of the

paroxysmal discharge (PD) followed by recurrent bursts (RBs) (Figure 7C), which likely reflect recurrent circuit activities in pilocarpine-treated hippocampal slices (Peret et al., 2014). Interestingly, the frequency power spectrogram (Figure 7C) revealed a marked reduction of power during RBs, but not PD, in *C1ql2/3*-null, as well as in *GluK2*-null DGCs. These results indicate that although pilocarpine induced MF sprouting, KARs were not recruited to *C1ql2/3*-null DGCs, and that the lack of postsynaptic KARs contributed to the reduction of recurrent burst activities.

To examine the pathological role of *C1ql2/3* *in vivo*, we next employed a pilocarpine-induced chronic epilepsy model in mice (Peret et al., 2014). One to two months after the occurrence of status epilepticus, we performed continuous video-electroencephalographic recording from the dentate gyrus of freely moving wild-type and *C1ql2/3*-null mice for 3 d. Although both genotypes displayed ictal discharges (Figure 7D) associated with generalized tonic-clonic seizures, the number of ictal events was significantly reduced in *C1ql2/3*-null mice (Figure 7E). IHC analysis revealed numerous ZnT3- and Bassoon-immunopositive sprouted MFs in both wild-type and *C1ql2/3*-null dentate gyrus (Figures 7F and S7A). Importantly, sprouted MF terminals in the dentate gyrus were immunopositive for *C1ql2* (Figure S7B) and colocalized with KARs (Figures 7F and S7C) in wild-type, but not in *C1ql2/3*-null dentate gyrus. Together, these results indicate that *C1ql2/3* originating from sprouted MFs recruit postsynaptic KARs in DGCs, contributing to recurrent circuit activities in the chronic epilepsy model *in vitro* and *in vivo* (Figure 7G).

## DISCUSSION

In this study, we showed that MF-derived *C1ql2* and *C1ql3* serve as extracellular organizers to

recruit functional postsynaptic KAR complexes, including Neto1 and high-affinity KAR subunits, to the CA3 pyramidal neurons (Figure 7G). C1ql2 and C1ql3 specifically bound the ATD of postsynaptic GluK2 and GluK4 KARs and the presynaptic Nr3+SS5<sup>25b</sup>. Considering that C1q-like proteins are expressed in multiple brain regions (Iijima et al., 2010; Miura et al., 2006), we propose that they are likely involved in recruitment and functional control of KARs at a broad variety of synapses. Our results suggest that C1q-like proteins serve as much broader feed-forward signals than previously appreciated, and impact directly on glutamatergic circuit formation and function, illustrating a novel, and possibly general, principle of iGluR regulation.

### **Presynaptically-derived anchors for postsynaptic targeting of iGluRs**

Precise targeting of specific iGluRs to the postsynaptic sites is crucial for the function of neuronal circuits. PSD-95 family proteins, such as PSD-93, PSD-95 and SAP-102, play essential roles in synaptic trafficking, stabilization and function of postsynaptic AMPA receptors and, to a lesser extent, NMDA receptors (Elias et al., 2006), by binding to the C-termini of transmembrane AMPA receptor regulatory proteins (TARPs) and GluN2 subunits, respectively. Similarly, postsynaptically enriched PDZ domain-containing proteins, such as GRIP, PICK1, syntenin and PSD-95, bind to the C-termini of KARs and play important roles in clustering and stabilizing them at postsynaptic sites (Hirbec et al., 2003; Pahl et al., 2014). Cell-adhesion transmembrane proteins, such as neuroligins and LRRTMs (de Wit et al., 2009; Ko et al., 2009; Siddiqui et al., 2010), bind to PSD-95 family proteins and are likely to be involved in recruiting them to synapses. However, it is not completely clear how PDZ proteins are targeted to specific postsynaptic sites to mediate the clustering of certain members of postsynaptic iGluRs (Elias and Nicoll, 2007). Indeed, the molecular mechanisms for the highly restricted expression of

postsynaptic KARs at MF–CA3 synapses has been unclear (Carta et al., 2014; Pahl et al., 2014).

Recruitment of postsynaptic receptors by presynaptically derived soluble factors represents alternative, or complementary, strategy to ensure their accumulation at a site apposed to its presynaptic counterpart. For example, agrin, a prototypical presynaptic protein at neuromuscular junctions, induces acetylcholine receptor clustering indirectly, by binding to the ectodomain of MuSK (Gautam et al., 1996). Recently, MADD-4B (punctin) was identified as a secreted anterograde organizer of GABAergic synapses through its binding to neuroligin and UNC-40 in *C. elegans* muscles (Maro et al., 2015; Tu et al., 2015). Neuronal pentraxins contribute to clustering and stabilizing postsynaptic AMPA receptors in parvalbumin-positive interneurons, binding mainly to the GluA4 subunit (Pelkey et al., 2015; Sia et al., 2007).

In contrast to the examples above, C1q family proteins are unique in that they are exclusively produced by specific presynaptic neurons, and appear to directly anchor postsynaptic receptors to presynaptic membranes. Parallel fibers secrete Cbln1 to accumulate and regulate the function of a postsynaptic iGluR member, GluD2, in cerebellar Purkinje cells through the direct binding (Matsuda et al., 2010; Uemura et al., 2010). We now report that C1ql2 and C1ql3, provided by MFs, recruit KARs in CA3 pyramidal neurons by directly binding to GluK2 and GluK4 KARs.

### **The role of iGluR ATDs**

The extracellular region of each iGluR subunit consists of one ATD and one ligand-binding domain (LBD), both of which belong to the periplasmic binding protein superfamily. Although the ATDs can make up nearly half of the full-length protein chains, their functional significance is not completely clear. The ATDs assist subtype-selective subunit assembly in AMPA receptors and KARs (Ayalon and Stern-Bach, 2001; Kumar et al., 2011; Rossmann et al., 2011) and

allosterically modify NMDA receptor channel activities (Gielen et al., 2009) (Karakas et al., 2011). An increasing number of soluble and transmembrane synaptic proteins are reported to bind iGluR ATDs. For example, neuronal pentraxins bind to GluA4 (Pelkey et al., 2015; Sia et al., 2007), N-cadherin binds to GluA2 (Saglietti et al., 2007), EphB binds to GluN1 (Dalva et al., 2000) and Cbln1 binds to GluD1 and GluD2 (Matsuda et al., 2010; Uemura et al., 2010). We have now demonstrated that C1ql2 and C1ql3 bind to the ATDs of GluA1, GluK2 and GluK4. These findings suggest that the ATDs of iGluRs, which extend ~13 nm away from the postsynaptic site (Karakas et al., 2015), is strategically suitable for interactions with synaptic proteins which regulate the positioning and thus function of iGluRs. We propose that yet unidentified synaptic proteins bind to the ATDs of all iGluR family members currently “orphan,” to modulate their functions at synapses. At least some of these unknown iGluR partners may belong to the C1q superfamily.

Although allosteric interactions between the ATD and LBD were demonstrated to date only for NMDA receptors, elastic network modeling indicate that AMPA and kainate receptor ectodomains could also adopt conformations linked to allosteric regulation (Dutta et al., 2015; Krieger et al., 2015). Indeed, although approximately half GluD2 is still localized at postsynaptic sites of the parallel fiber-Purkinje cell synapses in *Cbln1*-null cerebellum, the GluD2-dependent LTD is completely abolished in *Cbln1*-null mice (Hirai et al., 2005). Since D-Serine binding to the LBD of GluD2 activates downstream signaling to induce AMPA receptor endocytosis and LTD (Kakegawa et al., 2011), the failure to induce LTD in *Cbln1*-null Purkinje cells suggests that Nrx–Cbln1 binding to the ATD allosterically modulates the LBD response to D-Serine, to modulate GluD2 signaling at synapses. Thus, binding of Nrx–C1ql2/3 to the ATD of KARs, and perhaps binding of other synaptic molecules to iGluR ATDs, may not only modulate the location

of receptors, but is also likely to regulate iGluR signaling by restricting the range of relative LBD motions.

### **Nrx3 containing the SS5<sup>25b</sup> sequence binds C1q-like proteins**

Neurexins are encoded by three genes (*NRXN1–3* in human), each of whom uses two promoters to generate  $\alpha$  and  $\beta$  transcripts. Furthermore, alternative splicing of Nrx genes at six sites generates thousands of distinct isoforms in various brain regions (Schreiner et al., 2014; Treutlein et al., 2014). Such extensive variation in Nrx isoforms is thought to be used as a synapse-selective code to interact with distinct postsynaptic receptors. Indeed, the SS4 insert is crucial for Nrxs to bind to Cbln1 (Matsuda and Yuzaki, 2011; Uemura et al., 2010), whereas it blocks interaction of Nrxs with latrophilin and LRRTMs (Boucard et al., 2012; Ko et al., 2009) and may modulate the affinity of Nrxs to neuroligin isoforms (Boucard et al., 2005; Chih et al., 2006; Koehnke et al., 2010). However, whether other Nrx splicing sites play similar roles has remained unclear. Our finding that a sequence encoded by exon 25b in the splice site 5 of Nrx3 critically determines its binding affinity to C1ql2 and C1ql3 (Figure 4) suggests that there remain yet unidentified partners for Nrxs regulated by alternative splicing.

The sequence critical for binding to C1ql3 consists of 17 amino acids and is specific to Nrx3 (Figure S6). Interestingly, *NRXN3* single nucleotide polymorphisms (SNPs) are associated with addiction and obesity (Hishimoto et al., 2007; Lachman et al., 2007) and an SNP near the splice site 5 is shown to alter expression of Nrx3+SS5<sup>25b</sup> (Hishimoto et al., 2007). Furthermore, *de novo* and inherited deletions in *NRXN3* were reported for autism spectrum disorders (ASDs) (Vaags et al., 2012). Similarly, mutations in *GRIK2* gene encoding GluK2 were reported to be linked to ASDs (Jamain et al., 2002), intellectual disability and epilepsy (Cordoba et al., 2015; Motazacker

et al., 2007). We also demonstrated that C1ql2 and C1ql3 modulate synaptic network activities in a temporal lobe epilepsy model, as well as in control conditions, by regulating localization and function of postsynaptic KARs in the mouse hippocampus (Figure 7G). A detailed characterization of the molecular interaction networks involving Nrxs, C1q-like molecules and iGluRs is therefore essential for understanding and exploring new drug targets for neuropsychiatric and neurodevelopmental disorders.

## **EXPERIMENTAL PROCEDURES**

### **Animals**

*C1ql2*-null mice (TG0022) were purchased from Texas Institute for Genomic Medicine. *C1ql3*-floxed mice were generated by homologous recombination targeting exon 2 of *C1ql3* gene. *GluK2*-floxed mice were generated by homologous recombination targeting exon 14 of *Grik2* gene. To generate *C1ql3*-null or *GluK2*-null mice, the floxed mice were crossed with the telencephalin-*Cre* transgenic mice (Fuse et al., 2004). All procedures related to animal care and treatment were approved by the Animal Resource Committee of Keio University.

### **Preparation of Recombinant Proteins**

A hemagglutinin (HA)-tagged C1ql3 or C1ql2 protein was expressed in human embryonic kidney 293 tSA (HEK293) cells as described previously (Takegawa et al., 2015). The concentration of each recombinant HA-tagged C1ql3 and C1ql2 was quantified using an immunoblot analysis with purified histidine (His)-tagged HA-Cbln1 as a standard. His-tagged gC1ql1, gC1ql2 or gC1ql3 proteins, GluK-ATD or ectodomain of neurexin (Nrx) 3 $\beta$  for surface

plasmon resonance (SPR) assays were expressed in HEK293T cells as previously described (Aricescu et al., 2006).

### **Cell-based C1ql2/3 Binding Assays**

HEK293 cells transfected with pDisplay vectors containing myc-tagged iGluR ATDs or Flag-tagged Nr<sub>x</sub>3 constructs were incubated with equivalent concentrations (13–25 nM) of HA-tagged C1ql2, C1ql or Cbln1 for 4 h, fixed with 4% paraformaldehyde, and immunostained. The intensity of HA immunoreactivity within the myc-immunopositive cell area was quantified.

### **Primary Cultures**

Hippocampal cultures were prepared from embryonic day 17 to day-of-birth *C1ql2/3*-null mice as previously described (Matsuda et al., 2013) and co-cultured with HA-C1ql3 immobilized to avidin beads (Dyna) or HEK293 cells transfected with Nr<sub>x</sub>3β-Flag. The intensity of GluK2/3 immunoreactivity within segmented beads or Flag-immunopositive areas was quantified.

### **Surface Plasmon Resonance (SPR)**

SPR experiments were performed with streptavidin-coated CM5 chips using a Biacore T200 instrument (GE Healthcare). Proteins carrying a C-terminal Avitag were biotinylated using biotin ligase (BirA). Sensorgrams were analyzed using equilibrium and kinetics binding models.

### **Immunogold Electron Microscopy**

GluK2 or C1ql2 were labeled with gold-conjugated antibodies. The density of the immunogold particles per 100-nm length of postsynaptic densities on the electron micrographs was analyzed.

## **Electrophysiology**

Whole-cell voltage-clamp and extracellular field recordings were made in hippocampal slices from wild-type, *C1ql2/3*-null and *GluK2*-null mice at postnatal day (P)12–20. Excitatory postsynaptic currents were recorded from CA3 pyramidal cells and dentate gyrus granule cells.

## ***In vitro* Model of Temporal Lobe Epilepsy**

Brain slice cultures containing the hippocampus and the entorhinal cortex (350  $\mu$ m thickness) were prepared from *GluK2*-null, *C1ql2/3*-null and WT mice at P9–10 as previously described (Peret et al., 2014). Pilocarpine (0.5  $\mu$ M) was added to the medium at 5 days *in vitro* (DIV) and incubated for 2 d. Slices were used for experiments at 9–12 DIV.

## ***In vivo* Model of Temporal Lobe Epilepsy**

Scopolamine (2 mg/kg) was administered intraperitoneally (*i.p.*) 30 min before application of pilocarpine (250 mg/kg, *i.p.*) to age- and gender-matched *C1ql2/3*-null and wild-type mice at P60–90. Intra-hippocampal electroencephalographic (EEG) recordings were performed in freely-moving animals.

## **Data Analysis and Statistics**

All values are presented as the mean  $\pm$  SEM, and statistical significance between multiple groups was determined by Kruskal-Wallis test followed by Steel *post hoc* test, unless otherwise noted. Statistical significance between two groups with normal distribution was determined by Student t test. Statistical significance was assumed when  $p < 0.05$ .

## **SUPPLEMENTAL INFORMATION**

Supplemental Information includes six figures and Supplemental Experimental Procedures and can be found with this article online at: <http://xxxx>.

## **AUTHOR CONTRIBUTIONS**

K.M. designed the project, carried out the biochemical and anatomical works, analyzed the data and wrote the paper. T.B. and W.K. carried out the electrophysiological works and analyzed the data. N.M. and A.R.A. performed SPR analyses and designed constructs. M.K. and Y.S. supervised and performed EEG experiments. E.M., M.Y. and M.U. performed the anatomical experiments. K.K. performed in situ hybridization experiments. M.A., I.W. and K.S. generated and developed mutant mice. M.W. generated essential antibodies. M.Y. and A.R.A. designed and supervised the project and wrote the paper.

## **ACKNOWLEDGMENTS**

We thank S. Narumi, J. Motohashi and K. Suzuki for their technical assistance and M. Yamazaki and K. Akashi for production of *C1ql3*- and *GluK2*-null mice. We also thank H. Sakuma and T. Watanabe (Zeiss) for their support on super-resolution microscopy analysis. This work was supported by the Grant-in-Aid from the MEXT (K.M., T.B. and M.Y.), the CREST from the JST (M.Y.), the Keio Gijuku Fukuzawa Memorial Fund for the Advancement of Education and Research (K.M.), the Human Frontier Research Program (RGP0065/2014 to M.Y. and A.R.A.), the UK Medical Research Council (A.R.A.) and a Wellcome Trust D.Phil. studentship (N.M.). Further support from the Wellcome Trust Core Award Grant Number 090532/Z/09/Z is acknowledged. A.R.A. is an MRC Senior Research Fellow.

## FIGURE LEGENDS

### Figure 1. C1ql2 and C1ql3 are Localized at MF-CA3 Synapses.

(A) Endogenous C1ql2, C1ql3 and GluK2/3 immunoreactivities in wild-type (WT) hippocampus. Arrows indicate CA3 stratum lucidum. Insets show immunoreactivity in mice lacking a corresponding gene to confirm antibody specificity. Scale bar, 500  $\mu$ m.

(B) Representative IHC images indicating loss of C1ql2 and C1ql3 immunoreactivities (red) in *C1ql2-null* and *C1ql3-null* CA3 stratum lucidum, respectively. No differences in PSD95 (green) and MAP2 (blue) immunoreactivities among WT, *C1ql2-* and *C1ql3-null* mice. Scale bar, 10  $\mu$ m.

(C) Postembedding immunogold EM image of endogenous C1ql2 in WT MF–CA3 synapses. Red arrows indicate gold particles labelling C1ql2. sp, pyramidal cell spine; MF, mossy fiber terminal. Scale bar, 200 nm. Histogram shows distribution of C1ql2-positive particles at MF synapses in WT and *C1ql2/3-null* mice ( $n = 2$  mice each).

(D) Super-resolution structured illumination (SIM) microscopic images of endogenous C1ql2 (upper; red) or C1ql3 (lower; red), PSD95 (green) and Bassoon (white). Unfilled and filled triangles indicate presynaptic Bassoon-immunopositive and postsynaptic PSD95-immunopositive structures, respectively. Scale bar, 200 nm.

See also Figure S1.

### Figure 2. Direct Interaction between C1ql2/3 and ATDs of iGluRs.

(A) Cell-based binding assay. Diagram shows domain organization of iGluR. ATD, amino-terminal domain; LBD, ligand-binding domain; TMD, transmembrane domain; CTD, C-terminal domain. Panels show cell-surface C1ql2-HA (upper panels) or C1ql3-HA (lower

panels) immunoreactivity (red) on HEK293 cells expressing the ATD of iGluR-myc (green). Scale bars, 50  $\mu$ m.

(B) The graphs show mean HA immunoreactivity in the myc-positive area. HA immunoreactivity in HEK293 cells was compared with those expressing GluD2-ATD. At least  $n = 14$  fields were analyzed in two independent experiments. \*\*\* $p < 0.001$ .

(C, D) Reduction of synaptic C1ql2 and C1ql3 in *GluK2*-null and *GluK4*-null mice. Representative IHC images show endogenous C1ql2 (C; red) or C1ql3 (D; red) and PSD95 (green) immunoreactivities in wild-type (WT), *GluK2*-null, *GluK4*-null and double *C1ql2/3*-null hippocampus. Scale bars, 10  $\mu$ m. The graphs show relative fluorescence intensities of C1ql2 (C;  $n = 24$ –30 regions from 4–5 mice for each genotype) or C1ql3 (D;  $n = 12$  regions from 2 mice for each genotype) normalized by those of PSD95 in randomly selected CA3 regions. \*\*\* $p < 0.001$  vs. WT.

(E) Diagram of GluK (upper) and C1ql (lower) domain organization and construct design. N, amino-terminus; C, carboxy-terminus; SP, secretion signal peptide; Collagen-like, collagen-like region; gC1q, globular C1q domain. GluK numbering corresponds to rat proteins, C1ql numbering corresponds to mouse proteins.

(F) Surface plasmon resonance assay. The ATD of GluK2, but not GluK3 or GluK5, bound directly to gC1ql2 and gC1ql3.

Data are presented as mean  $\pm$  SEM. See also Figures S2 and S3.

### **Figure 3. C1ql2 and C1ql3 Determine Postsynaptic KAR Localization at MF-CA3 Synapses.**

(A) Absence of synaptic GluK2/3 in *C1ql2/3*-null hippocampus. Representative IHC images show endogenous GluK2/3 (red), PSD95 (green) and MAP2 (green or blue) immunoreactivities in

wild-type (WT), *Clql2/3*-null and *GluK2*-null CA3 regions. The boxed regions are enlarged in the right panels. Scale bars, 100  $\mu$ m (left) and 20  $\mu$ m (right). The graph shows relative fluorescence intensities of GluK2/3 normalized by those of PSD95 in randomly selected CA3 regions ( $n = 24$ –30 regions from 4–5 mice for each genotype). \*\*\* $p < 0.001$  vs. WT.

(B) Postembedding immunogold EM images of endogenous GluK2/3 (arrows) at MF–CA3 synapses in WT, *Clql2/3*-null and *GluK2*-null hippocampus. sp, pyramidal cell spine; MF, mossy fiber terminal. Scale bar, 200 nm. The mean number of gold particle per 100 nm of postsynaptic density (PSD) (left graph) and the length of PSD (right graph) are summarized. \*\*\* $p < 0.001$  vs. WT. n.s, no significance. ( $n > 100$  synapses from 2 mice for each genotype).

(C) Representative immunoblot image indicating no difference in total GluK2/3 proteins between WT and *Clql2/3*-null hippocampal CA3 regions. CA3 regions were excised and subjected to the immunoblot analyses using anti-GluK2/3 and anti-calbindin (an MF marker) antibodies. The lower graph shows averaged GluK2/3 band intensities normalized by those of calbindin. n.s, no significance vs. WT. ( $n = 3$  from 3 mice for each genotype).

(D) Reduced Neto1 immunoreactivity in *Clql2/3*-null, but not in WT, *Clql2*-null or *Clql3*-null hippocampus. Bottom panels show enlarged views of CA3 stratum lucidum. Scale bars, 100  $\mu$ m (top) and 20  $\mu$ m (bottom). The middle graph shows relative fluorescence intensities of Neto1 normalized by those of PSD95 in randomly selected CA3 regions ( $n = 8$  regions from 4 mice for each genotype). \*\* $p < 0.01$ ; n.s, no significance by Kruskal-Wallis test and Steel-Dwass *post hoc* test. Cumulative plot of Neto1 immunoreactivity on PSD95 immunopositive puncta is shown on the right.

(E) Loss of synaptic high-affinity KARs. Representative IHC images show GluK4 (upper) or GluK5 (lower) immunoreactivities in *Clql2/3*-null and *GluK2*-null CA3 stratum lucidum. Scale

bar, 10  $\mu$ m. The graphs show averaged GluK4 (left;  $n = 12$ – $17$  regions from 3 mice for each genotype) or GluK5 (right,  $n = 24$ – $30$  regions from 4–5 mice for each genotype) immunoreactivities normalized by those of PSD95 in randomly selected CA3 regions.

Data are presented as mean  $\pm$  SEM. See also Figures S4 and S5.

**Figure 4. Direct Interaction between C1ql2/3 and Nr $\alpha$ 3+SS5<sup>25b</sup>.**

(A) Diagram of domain organization of neurexin (Nr $\alpha$ ) isoforms and construct design. N, amino-terminus; C, carboxy-terminus; SS4, splice site 4; SS5, splice site 5; light green boxes, LNS (laminin, neurexin, sex-hormone binding protein) domain 1–6; yellow boxes, Nr $\alpha$  $\beta$ -specific region.

(B) Enzyme-linked immuno-sorbent assay showing interaction of Nr $\alpha$ 3 $\beta$  with C1ql2, C1ql3 or Cbln1. HA-C1ql2, C1ql3 or Cbln1 was incubated with HEK293 cells expressing various Nr $\alpha$  isoforms, followed by an anti-HA antibody and peroxidase-conjugated secondary antibody. The graph shows intensities of peroxidase reaction in HEK293 cells. Data are from 10 independent experiments. \*\* $p < 0.01$ ; n.s, no significance, by Kruskal-Wallis test and Steel-Dwass *post hoc* test.

(C, D) Cell-based binding assay showing that a sequence encoded by exon 25b, but not  $\beta$ -specific exon 18, determines binding specificity of Nr $\alpha$ 3 $\beta$  to C1ql3. Panels (C) show cell-surface HA-C1ql3 immunoreactivity (red) in HEK293 cells expressing various isoforms of Flag-tagged Nr $\alpha$  or GFP alone (green). Scale bar, 100  $\mu$ m. The graph (D) shows mean HA immunoreactivity in the Flag-positive area. At least  $n = 16$  fields were analyzed in two independent experiments. \*\*\* $p < 0.001$ ; n.s, no significance by Kruskal-Wallis test and Steel-Dwass *post hoc* test.

(E) Diagram of Nr $\alpha$ 3 $\beta$  ectodomain (ect-Nr $\alpha$ 3 $\beta$ ) and C1q-like proteins. SP, secretion signal

peptide; SS4, SS5, splice site 4 and 5; LNS6, LNS6 common to both  $\text{Nr}\alpha$  and  $\text{Nr}\beta$ ; gC1q, global C1q domain. The core 17 amino-acid sequence within the region encoded by exon 25b ( $\text{SS5}^{25b}$ ) is referred to as S5-9. Numbering corresponds to mouse proteins.

(F) Equilibrium SPR analysis of binding between  $\text{ect-Nr}\beta 3\beta \pm \text{SS5}^{25b}$  and immobilized gC1q2 and gC1q3. The  $\text{ect-Nr}\beta 3\beta + \text{SS5}^{25b}$ , but not  $-\text{SS5}^{25b}$ , bound to gC1q2 and gC1q3.

(G) Equilibrium SPR analysis of binding between gC1q3 and immobilized peptide S5-9. Peptide S5-9 bound directly to gC1q3.

(H) Equilibrium SPR analysis of binding between  $\text{ect-Nr}\beta 3\beta \pm \text{SS5}^{25b}$  and immobilized full-length C1q2 (C1q2 FL). The  $\text{ect-Nr}\beta 3\beta + \text{SS5}^{25b}$  bound to C1q2 FL with a higher affinity than  $\text{ect-Nr}\beta 3\beta - \text{SS5}^{25b}$  did

Data are presented as mean  $\pm$  SEM. See also Figure S6.

### **Figure 5. $\text{Nr}\beta 3\beta$ –C1q2/3 Signaling Recruits KARs in Cultured Hippocampal Neurons.**

(A, B) HEK293 cells coexpressing C1q2, C1q3 and  $\text{Nr}\beta 3\beta$  recruit KARs in *C1ql2/3*-null hippocampal neurons. HEK293 cells expressing Flag-tagged  $\text{Nr}\beta 3\beta$  containing  $\text{SS5}^{25b}$  ( $\text{Nr}\beta 3\beta + \text{SS5}^{25b}$ ; green) were cocultured with *C1ql2/3*-null hippocampal neurons. Panels in (A) show accumulation of NL1 (left) and PSD95 (right) immunoreactivities (blue) in juxtaposed hippocampal neurons. GluK2/3 immunoreactivity (red) clustered only when C1q2 and C1q3 (C1q2+3) were coexpressed in HEK293 cells. Panels in (B) show that HEK293 cells expressing  $\text{Nr}\beta 3\beta$  lacking the LNS6 domain ( $\text{Nr}\beta 3\beta + \text{SS5}^{25b} \Delta \text{LNS}$ ) accumulated GluK2/3 (red), but not NL1 (blue), immunoreactivities in hippocampal neurons. Scale bar, 25  $\mu\text{m}$ .

(C) HEK293 cells coexpressing  $\text{Nr}\beta 3\beta + \text{SS5}^{25b}$  and either C1q2 or C1q3 recruit KARs in *C1ql2/3*-null hippocampal neurons. Panels show accumulation of GluK2/3 immunoreactivity

(red) in hippocampal neurons juxtaposed to HEK293 cells coexpressing Nr3 $\beta$ +SS5<sup>25b</sup> (green) and either C1ql2 or C1ql3. Scale bar, 25  $\mu$ m. The graph shows the mean GluK2/3 immunoreactivity accumulated around HEK 293 cells. At least  $n > 100$  cells were analyzed from two independent experiments. \*\*\* $p < 0.001$  by Kruskal-Wallis test and Scheffe *post hoc* test.

(D) C1ql3 directly serves as a synaptic organizer for KARs. Beads coated with HA-C1ql3, but not uncoated beads (control), accumulated GluK2/3 immunoreactivity (red) in *C1ql2/3*-null cultured hippocampal neurons. Scale bar, 20  $\mu$ m. The graph shows the mean GluK2/3 immunoreactivity on the beads. At least  $n > 300$  beads were analyzed from two independent experiments. \*\*\* $p < 0.001$  by Mann-Whitney *U* test. Data are presented as mean  $\pm$  SEM.

### **Figure 6. C1ql2/3 Determine Postsynaptic KAR Functions in the Hippocampus.**

(A) Loss of postsynaptic KAR-mediated EPSCs in *C1ql2/3*-null hippocampus. MF-evoked EPSCs were recorded in the absence and presence of 60  $\mu$ M GYKI52466 (GYKI) combined with 25  $\mu$ M D-AP-5 (blue lines) to evaluate KAR-mediated EPSCs in wild-type (WT; black,  $n = 19$  from 7 mice), *C1ql2/3*-null (red,  $n = 13$  from 6 mice) or *GluK2*-null (green,  $n = 9$  from 4 mice) CA3 neurons at  $-70$  mV. The top graph shows mean amplitudes of GYKI-resistant MF-EPSCs. Lower enlarged traces show slowly decaying GYKI-resistant MF-EPSCs in WT, but not in *C1ql2/3*-null or *GluK2*-null CA3 neurons. The bottom graph shows the mean ratio of decay time constants before and after application of GYKI. \* $p < 0.05$  vs. WT by one-way ANOVA followed by Bonferroni *post hoc* analysis.

(B) C1ql2/3 modulate KAR-mediated summation of MF-EPSCs. Representative traces show that MF stimulation at 20 Hz for 5 times in the presence of GYKI (100  $\mu$ M) and D-AP5 (25  $\mu$ M) evoked EPSC summation in WT (black,  $n = 11$  from 3 mice), but not in *C1ql2/3*-null (red,  $n = 11$

from 3 mice), CA3 pyramidal neurons.

(C) *C1ql2/3* modulate likelihood of action potential initiation during repetitive MF stimulation. Representative EPSP traces show that MF stimulation at 20 Hz for five times resulted in action potential generation in WT (black,  $n = 11$  from 4 mice), but not in *C1ql2/3*-null (red,  $n = 10$  from 4 mice), CA3 pyramidal neurons. The graph shows spiking probability plotted against the number of MF stimulation. \* $p < 0.05$  by Mann-Whitney  $U$  test.

(D) No changes in postsynaptic AMPARs. Representative traces show asynchronous MF-evoked EPSCs in WT (black,  $n = 7$  cells) and *C1ql2/3*-null (red,  $n = 9$  cells) CA3 pyramidal neurons clamped at  $-80$  mV in the presence of 8 mM  $\text{Sr}^{2+}$ , 50  $\mu\text{M}$  D-AP5 and 5  $\mu\text{M}$  UBP310. Averaged asynchronous EPSCs (aEPSCs, bottom) indicate no differences in the amplitude and kinetics. The graph shows cumulative plot of aEPSCs in WT (black) and *C1ql2/3*-null CA3 neurons (red).

(E) No changes in the postsynaptic AMPA/NMDA ratio. MF-evoked EPSCs were recorded at  $-80$  mV (thick lines) to estimate AMPAR-mediated components and at  $+40$  mV in the presence of 20  $\mu\text{M}$  CNQX (thin lines) to evaluate NMDAR components in WT ( $n = 8$ ) and *C1ql2/3*-null ( $n = 9$ ) CA3 pyramidal neurons. The graph shows averaged AMPA/NMDA ratio in each genotype. \* $p < 0.05$  by Mann-Whitney  $U$  test.

(F) Normal presynaptic KAR functions at *C1ql2/3*-null MF-CA3 synapses. Representative traces show that MF-EPSCs at inter-stimulus interval of 50 ms were inhibited by 3  $\mu\text{M}$  kainate (orange) in WT (black,  $n = 7$  from 3 mice) and *C1ql2/3*-null (red,  $n = 10$  from 4 mice), but not in *GluK2*-null (green,  $n = 7$  from 3 mice), CA3 pyramidal neurons in the presence of 25  $\mu\text{M}$  D-AP-5. The graphs show the percentages of kainate-induced reduction of amplitudes (top) and the paired-pulse facilitation ratio (PPR; bottom) of MF-EPSCs. \* $p < 0.05$  vs. WT, n.s, no significance, by one-way ANOVA followed by Bonferroni *post hoc* analysis.

Data are presented as mean  $\pm$  SEM.

**Figure 7. C1ql2/3 Regulate Postsynaptic Localization of KARs in Sprouted MFs and Contribute to Recurrent Circuit Activities in Chronic Epilepsy Models.**

(A-C) *In vitro* model.

(A) The representative IHC image shows similar levels of sprouted recurrent MF terminals (rMF) immunopositive for synaptoporin (red) and DAPI (blue) in the granular layer of the dentate gyrus (gl, dotted lines) in wild-type (WT) and *C1ql2/3*-null cultured hippocampal slices treated with pilocarpine. The boxed regions are enlarged in the bottom. Scale bar, 100  $\mu$ m.

(B) Spontaneous EPSCs recorded from WT (black,  $n = 19$  slices), but not *C1ql2/3*-null (red,  $n = 38$  slices), DGCs show KAR-mediated components. Holding potential,  $-80$  mV. Asterisks indicate slow representative KAR-mediated EPSCs, which were resistant to 60  $\mu$ M GYKI52466 and 50  $\mu$ M D-AP-5 (lower traces).

(C) Extracellular field recordings of spontaneous epileptiform activity in the dentate gyrus (in ACSF containing 5 mM  $K^+$  and 100  $\mu$ M picrotoxin) from WT (black,  $n = 42$  slices), *C1ql2/3*-null (red,  $n = 32$  slices) or *GluK2*-null slices (green,  $n = 28$  slices). Interictal-like activity consists of paroxysmal discharge (PD) followed by recurrent bursts (RBs). High-pass filtered ( $>100$  Hz) traces are shown in the bottom. Graphs show power spectrum analysis of filtered RBs (left), maximum power of RBs (middle) and PDs (right) in each group.  $*p < 0.05$  vs. WT by one-way ANOVA followed by Bonferroni *post hoc* analysis.

(D-F) *In vivo* model.

(D) Typical ictal traces recorded from the dentate gyrus of pilocarpine-treated WT (black) and *C1ql2/3*-null (red) mice.

(E) Number of ictal events in WT ( $n = 9$ ) and *C1ql2/3*-null mice ( $n = 8$ ) per 72 h. \* $p < 0.05$  by Mann-Whitney  $U$  test.

(F) Sprouted MFs do not recruit GluK5 in *C1ql2/3*-null hippocampus. IHC analyses show sprouted MF terminals immunopositive for ZnT3 (green) and Bassoon (Bsn; blue) in the supra-granular layer of the dentate gyrus of pilocarpine-treated mice. GluK5 immunoreactivity (red) colocalized with ZnT3-positive MF terminals in WT, but not in *C1ql2/3*-null, dentate gyrus. Granule layer is indicated by dotted lines (gl). Scale bar, 25  $\mu\text{m}$ . The right graph shows mean GluK5 fluorescence intensities on ZnT3-immunopositive MF terminals. \*\*\* $p < 0.001$ .  $n = 9$  from 3 mice for each genotype. Data are presented as mean  $\pm$  SEM.

(G) Proposed molecular model leading to trans-synaptic modulation of kainite receptor function by neurexin and C1ql proteins.

See also Figure S7.

## REFERENCES

- Akashi, K., Kakizaki, T., Kamiya, H., Fukaya, M., Yamasaki, M., Abe, M., Natsume, R., Watanabe, M., and Sakimura, K. (2009). NMDA receptor GluN2B (GluR epsilon 2/NR2B) subunit is crucial for channel function, postsynaptic macromolecular organization, and actin cytoskeleton at hippocampal CA3 synapses. *J. Neurosci.* 29, 10869-10882.
- Aricescu, A.R., Lu, W., and Jones, E.Y. (2006). A time- and cost-efficient system for high-level protein production in mammalian cells. *Acta Crystallogr. D Biol. Crystallogr.* 62, 1243-1250.
- Ayalon, G., and Stern-Bach, Y. (2001). Functional assembly of AMPA and kainate receptors is mediated by several discrete protein-protein interactions. *Neuron* 31, 103-113.
- Bolliger, M.F., Martinelli, D.C., and Sudhof, T.C. (2011). The cell-adhesion G protein-coupled receptor BAI3 is a high-affinity receptor for C1q-like proteins. *Proc. Natl. Acad. Sci. USA* 108, 2534-2539.
- Boucard, A.A., Chubykin, A.A., Comoletti, D., Taylor, P., and Sudhof, T.C. (2005). A splice code for trans-synaptic cell adhesion mediated by binding of neuroligin 1 to alpha- and beta-neurexins. *Neuron* 48, 229-236.
- Boucard, A.A., Ko, J., and Sudhof, T.C. (2012). High affinity neurexin binding to cell adhesion G-protein-coupled receptor CIRL1/latrophilin-1 produces an intercellular adhesion complex. *J. Biol. Chem.* 287, 9399-9413.
- Carta, M., Fiebre, S., Gorlewicz, A., and Mulle, C. (2014). Kainate receptors in the hippocampus. *Eur. J. Neurosci.* 39, 1835-1844.
- Castillo, P.E., Malenka, R.C., and Nicoll, R.A. (1997). Kainate receptors mediate a slow postsynaptic current in hippocampal CA3 neurons. *Nature* 388, 182-186.
- Chih, B., Gollan, L., and Scheiffele, P. (2006). Alternative splicing controls selective trans-synaptic interactions of the neuroligin-neurexin complex. *Neuron* 51, 171-178.
- Contractor, A., Mulle, C., and Swanson, G.T. (2011). Kainate receptors coming of age: milestones of two decades of research. *Trends Neurosci.* 34, 154-163.
- Contractor, A., Swanson, G.T., Sailer, A., O'Gorman, S., and Heinemann, S.F. (2000). Identification of the kainate receptor subunits underlying modulation of excitatory synaptic transmission in the CA3 region of the hippocampus. *J. Neurosci.* 20, 8269-8278.
- Copits, B.A., and Swanson, G.T. (2012). Dancing partners at the synapse: auxiliary subunits that shape kainate receptor function. *Nat. Rev. Neurosci.* 13, 675-686.
- Cordoba, M., Rodriguez, S., Gonzalez Moron, D., Medina, N., and Kauffman, M.A. (2015). Expanding the spectrum of Grik2 mutations: intellectual disability, behavioural disorder, epilepsy and dystonia. *Clin Genet* 87, 293-295.

Dalva, M.B., Takasu, M.A., Lin, M.Z., Shamah, S.M., Hu, L., Gale, N.W., and Greenberg, M.E. (2000). EphB receptors interact with NMDA receptors and regulate excitatory synapse formation. *Cell* 103, 945-956.

de Wit, J., Sylwestrak, E., O'Sullivan, M.L., Otto, S., Tiglio, K., Savas, J.N., Yates, J.R., 3rd, Comoletti, D., Taylor, P., and Ghosh, A. (2009). LRRTM2 interacts with Neurexin1 and regulates excitatory synapse formation. *Neuron* 64, 799-806.

Dutta, A., Krieger, J., Lee, J.Y., Garcia-Nafria, J., Greger, I.H., and Bahar, I. (2015). Cooperative Dynamics of Intact AMPA and NMDA Glutamate Receptors: Similarities and Subfamily-Specific Differences. *Structure*.

Elias, G.M., Funke, L., Stein, V., Grant, S.G., Brecht, D.S., and Nicoll, R.A. (2006). Synapse-specific and developmentally regulated targeting of AMPA receptors by a family of MAGUK scaffolding proteins. *Neuron* 52, 307-320.

Elias, G.M., and Nicoll, R.A. (2007). Synaptic trafficking of glutamate receptors by MAGUK scaffolding proteins. *Trends Cell Biol.* 17, 343-352.

Fuse, T., Kanai, Y., Kanai-Azuma, M., Suzuki, M., Nakamura, K., Mori, H., Hayashi, Y., and Mishina, M. (2004). Conditional activation of RhoA suppresses the epithelial to mesenchymal transition at the primitive streak during mouse gastrulation. *Biochem. Biophys. Res. Commun.* 318, 665-672.

Gautam, M., Noakes, P.G., Moscoso, L., Rupp, F., Scheller, R.H., Merlie, J.P., and Sanes, J.R. (1996). Defective neuromuscular synaptogenesis in agrin-deficient mutant mice. *Cell* 85, 525-535.

Gielen, M., Siegler Retchless, B., Mony, L., Johnson, J.W., and Paoletti, P. (2009). Mechanism of differential control of NMDA receptor activity by NR2 subunits. *Nature* 459, 703-707.

Gokce, O., and Sudhof, T.C. (2013). Membrane-tethered monomeric neurexin LNS-domain triggers synapse formation. *J. Neurosci.* 33, 14617-14628.

Grabs, D., Bergmann, M., Schuster, T., Fox, P.A., Brich, M., and Gratz, M. (1994). Differential expression of synaptophysin and synaptoporin during pre- and postnatal development of the rat hippocampal network. *Eur. J. Neurosci.* 6, 1765-1771.

Hardingham, G.E., and Bading, H. (2010). Synaptic versus extrasynaptic NMDA receptor signalling: implications for neurodegenerative disorders. *Nat. Rev. Neurosci.* 11, 682-696.

Hirai, H., Pang, Z., Bao, D., Miyazaki, T., Li, L., Miura, E., Parris, J., Rong, Y., Watanabe, M., Yuzaki, M., *et al.* (2005). Cbln1 is essential for synaptic integrity and plasticity in the cerebellum. *Nat. Neurosci.* 8, 1534-1541.

Hirbec, H., Francis, J.C., Lauri, S.E., Braithwaite, S.P., Coussen, F., Mulle, C., Dev, K.K., Coutinho, V., Meyer, G., Isaac, J.T., *et al.* (2003). Rapid and differential regulation of AMPA and kainate receptors at hippocampal mossy fibre synapses by PICK1 and GRIP. *Neuron* 37,

625-638.

Hishimoto, A., Liu, Q.R., Drgon, T., Pletnikova, O., Walther, D., Zhu, X.G., Troncoso, J.C., and Uhl, G.R. (2007). Neurexin 3 polymorphisms are associated with alcohol dependence and altered expression of specific isoforms. *Hum. Mol. Genet.* *16*, 2880-2891.

Iijima, T., Miura, E., Watanabe, M., and Yuzaki, M. (2010). Distinct expression of C1q-like family mRNAs in mouse brain and biochemical characterization of their encoded proteins. *Eur. J. Neurosci.* *31*, 1606-1615.

Jamain, S., Betancur, C., Quach, H., Philippe, A., Fellous, M., Giros, B., Gillberg, C., Leboyer, M., Bourgeron, T., and Paris Autism Research International Sibpair, S. (2002). Linkage and association of the glutamate receptor 6 gene with autism. *Mol. Psychiatry* *7*, 302-310.

Kakegawa, W., Mitakidis, N., Miura, E., Abe, M., Matsuda, K., Takeo, Y.H., Kohda, K., Motohashi, J., Takahashi, A., Nagao, S., *et al.* (2015). Anterograde C1ql1 signaling is required in order to determine and maintain a single-winner climbing fiber in the mouse cerebellum. *Neuron* *85*, 316-329.

Kakegawa, W., Miyoshi, Y., Hamase, K., Matsuda, S., Matsuda, K., Kohda, K., Emi, K., Motohashi, J., Konno, R., Zaitzu, K., *et al.* (2011). D-serine regulates cerebellar LTD and motor coordination through the delta2 glutamate receptor. *Nat. Neurosci.* *14*, 603-611.

Kamiya, H., and Ozawa, S. (2000). Kainate receptor-mediated presynaptic inhibition at the mouse hippocampal mossy fibre synapse. *J. Physiol.* *523 Pt 3*, 653-665.

Karakas, E., Regan, M.C., and Furukawa, H. (2015). Emerging structural insights into the function of ionotropic glutamate receptors. *Trends Biochem. Sci.* *40*, 328-337.

Karakas, E., Simorowski, N., and Furukawa, H. (2011). Subunit arrangement and phenylethanolamine binding in GluN1/GluN2B NMDA receptors. *Nature* *475*, 249-253.

Kishore, U., Gaboriaud, C., Waters, P., Shrive, A.K., Greenhough, T.J., Reid, K.B., Sim, R.B., and Arlaud, G.J. (2004). C1q and tumor necrosis factor superfamily: modularity and versatility. *Trends Immunol.* *25*, 551-561.

Ko, J., Fuccillo, M.V., Malenka, R.C., and Sudhof, T.C. (2009). LRRTM2 functions as a neurexin ligand in promoting excitatory synapse formation. *Neuron* *64*, 791-798.

Koehnke, J., Katsamba, P.S., Ahlsen, G., Bahna, F., Vendome, J., Honig, B., Shapiro, L., and Jin, X. (2010). Splice form dependence of beta-neurexin/neuroligin binding interactions. *Neuron* *67*, 61-74.

Kohda, K., Kakegawa, W., Matsuda, S., Yamamoto, T., Hirano, H., and Yuzaki, M. (2013). The delta2 glutamate receptor gates long-term depression by coordinating interactions between two AMPA receptor phosphorylation sites. *Proc. Natl. Acad. Sci. USA* *110*, E948-957.

Krieger, J., Bahar, I., and Greger, I.H. (2015). Structure, Dynamics, and Allosteric Potential of

Ionotropic Glutamate Receptor N-Terminal Domains. *Biophys. J.*

Kumar, J., Schuck, P., and Mayer, M.L. (2011). Structure and assembly mechanism for heteromeric kainate receptors. *Neuron* 71, 319-331.

Lachman, H.M., Fann, C.S., Bartzis, M., Evgrafov, O.V., Rosenthal, R.N., Nunes, E.V., Miner, C., Santana, M., Gaffney, J., Riddick, A., *et al.* (2007). Genomewide suggestive linkage of opioid dependence to chromosome 14q. *Hum. Mol. Genet.* 16, 1327-1334.

Lerma, J., and Marques, J.M. (2013). Kainate receptors in health and disease. *Neuron* 80, 292-311.

Maro, G.S., Gao, S., Olechwier, A.M., Hung, W.L., Liu, M., Ozkan, E., Zhen, M., and Shen, K. (2015). MADD-4/Punctin and Neurexin Organize *C. elegans* GABAergic Postsynapses through Neuroligin. *Neuron* 86, 1420-1432.

Matsuda, K., Miura, E., Miyazaki, T., Kakegawa, W., Emi, K., Narumi, S., Fukazawa, Y., Ito-Ishida, A., Kondo, T., Shigemoto, R., *et al.* (2010). Cbln1 is a ligand for an orphan glutamate receptor delta2, a bidirectional synapse organizer. *Science* 328, 363-368.

Matsuda, K., and Yuzaki, M. (2011). Cbln family proteins promote synapse formation by regulating distinct neurexin signaling pathways in various brain regions. *Eur. J. Neurosci.* 33, 1447-1461.

Matsuda, S., Kakegawa, W., Budisantoso, T., Nomura, T., Kohda, K., and Yuzaki, M. (2013). Stargazin regulates AMPA receptor trafficking through adaptor protein complexes during long-term depression. *Nat. Commun.* 4, 2759.

Miura, E., Iijima, T., Yuzaki, M., and Watanabe, M. (2006). Distinct expression of Cbln family mRNAs in developing and adult mouse brains. *Eur. J. Neurosci.* 24, 750-760.

Motazacker, M.M., Rost, B.R., Hucho, T., Garshasbi, M., Kahrizi, K., Ullmann, R., Abedini, S.S., Nieh, S.E., Amini, S.H., Goswami, C., *et al.* (2007). A defect in the ionotropic glutamate receptor 6 gene (GRIK2) is associated with autosomal recessive mental retardation. *Am. J. Hum. Genet.* 81, 792-798.

Pahl, S., Tapken, D., Haering, S.C., and Hollmann, M. (2014). Trafficking of kainate receptors. *Membranes (Basel)* 4, 565-595.

Pelkey, K.A., Barksdale, E., Craig, M.T., Yuan, X., Sukumaran, M., Vargish, G.A., Mitchell, R.M., Wyeth, M.S., Petralia, R.S., Chittajallu, R., *et al.* (2015). Pentraxins coordinate excitatory synapse maturation and circuit integration of parvalbumin interneurons. *Neuron* 85, 1257-1272.

Peret, A., Christie, L.A., Ouedraogo, D.W., Gorlewicz, A., Epsztein, J., Mulle, C., and Crepel, V. (2014). Contribution of aberrant GluK2-containing kainate receptors to chronic seizures in temporal lobe epilepsy. *Cell Rep.* 8, 347-354.

Petralia, R.S., Wang, Y.X., and Wenthold, R.J. (1994). Histological and ultrastructural

localization of the kainate receptor subunits, KA2 and GluR6/7, in the rat nervous system using selective antipeptide antibodies. *J. Comp. Neurol.* **349**, 85-110.

Rossmann, M., Sukumaran, M., Penn, A.C., Veprintsev, D.B., Babu, M.M., and Greger, I.H. (2011). Subunit-selective N-terminal domain associations organize the formation of AMPA receptor heteromers. *EMBO J.* **30**, 959-971.

Saglietti, L., Dequidt, C., Kamieniarz, K., Rousset, M.C., Valnegri, P., Thoumine, O., Beretta, F., Fagni, L., Choquet, D., Sala, C., *et al.* (2007). Extracellular interactions between GluR2 and N-cadherin in spine regulation. *Neuron* **54**, 461-477.

Schreiner, D., Nguyen, T.M., Russo, G., Heber, S., Patrignani, A., Ahrne, E., and Scheiffele, P. (2014). Targeted combinatorial alternative splicing generates brain region-specific repertoires of neurexins. *Neuron* **84**, 386-398.

Schwenk, J., Harmel, N., Brechet, A., Zolles, G., Berkefeld, H., Muller, C.S., Bildl, W., Baehrens, D., Huber, B., Kulik, A., *et al.* (2012). High-resolution proteomics unravel architecture and molecular diversity of native AMPA receptor complexes. *Neuron* **74**, 621-633.

Shanks, N.F., Savas, J.N., Maruo, T., Cais, O., Hirao, A., Oe, S., Ghosh, A., Noda, Y., Greger, I.H., Yates, J.R., 3rd, *et al.* (2012). Differences in AMPA and kainate receptor interactomes facilitate identification of AMPA receptor auxiliary subunit GSG1L. *Cell Rep.* **1**, 590-598.

Shimono, C., Manabe, R., Yamada, T., Fukuda, S., Kawai, J., Furutani, Y., Tsutsui, K., Ikenaka, K., Hayashizaki, Y., and Sekiguchi, K. (2010). Identification and characterization of nCLP2, a novel C1q family protein expressed in the central nervous system. *J. Biochem.* **147**, 565-579.

Sia, G.M., Beique, J.C., Rumbaugh, G., Cho, R., Worley, P.F., and Huganir, R.L. (2007). Interaction of the N-terminal domain of the AMPA receptor GluR4 subunit with the neuronal pentraxin NP1 mediates GluR4 synaptic recruitment. *Neuron* **55**, 87-102.

Siddiqui, T.J., Pancaroglu, R., Kang, Y., Rooyakkers, A., and Craig, A.M. (2010). LRRTMs and neuroligins bind neurexins with a differential code to cooperate in glutamate synapse development. *J. Neurosci.* **30**, 7495-7506.

Straub, C., Hunt, D.L., Yamasaki, M., Kim, K.S., Watanabe, M., Castillo, P.E., and Tomita, S. (2011). Distinct functions of kainate receptors in the brain are determined by the auxiliary subunit Neto1. *Nat. Neurosci.* **14**, 866-873.

Tang, M., Pelkey, K.A., Ng, D., Ivakine, E., McBain, C.J., Salter, M.W., and McInnes, R.R. (2011). Neto1 is an auxiliary subunit of native synaptic kainate receptors. *J. Neurosci.* **31**, 10009-10018.

Traynelis, S.F., Wollmuth, L.P., McBain, C.J., Menniti, F.S., Vance, K.M., Ogden, K.K., Hansen, K.B., Yuan, H., Myers, S.J., and Dingledine, R. (2010). Glutamate receptor ion channels: structure, regulation, and function. *Pharmacol. Rev.* **62**, 405-496.

Treutlein, B., Gokce, O., Quake, S.R., and Sudhof, T.C. (2014). Cartography of neurexin

alternative splicing mapped by single-molecule long-read mRNA sequencing. *Proc. Natl. Acad. Sci. USA* *111*, E1291-1299.

Tu, H., Pinan-Lucarre, B., Ji, T., Jospin, M., and Bessereau, J.L. (2015). *C. elegans* Punctin Clusters GABAA Receptors via Neuroligin Binding and UNC-40/DCC Recruitment. *Neuron* *86*, 1407-1419.

Uemura, T., Lee, S.J., Yasumura, M., Takeuchi, T., Yoshida, T., Ra, M., Taguchi, R., Sakimura, K., and Mishina, M. (2010). Trans-synaptic interaction of GluRdelta2 and Neurexin through Cbln1 mediates synapse formation in the cerebellum. *Cell* *141*, 1068-1079.

Vaags, A.K., Lionel, A.C., Sato, D., Goodenberger, M., Stein, Q.P., Curran, S., Ogilvie, C., Ahn, J.W., Drmic, I., Senman, L., *et al.* (2012). Rare deletions at the neurexin 3 locus in autism spectrum disorder. *Am. J. Hum. Genet.* *90*, 133-141.

Yuzaki, M. (2008). Cbln and C1q family proteins: new transneuronal cytokines. *Cell. Mol. Life Sci.* *65*, 1698-1705.

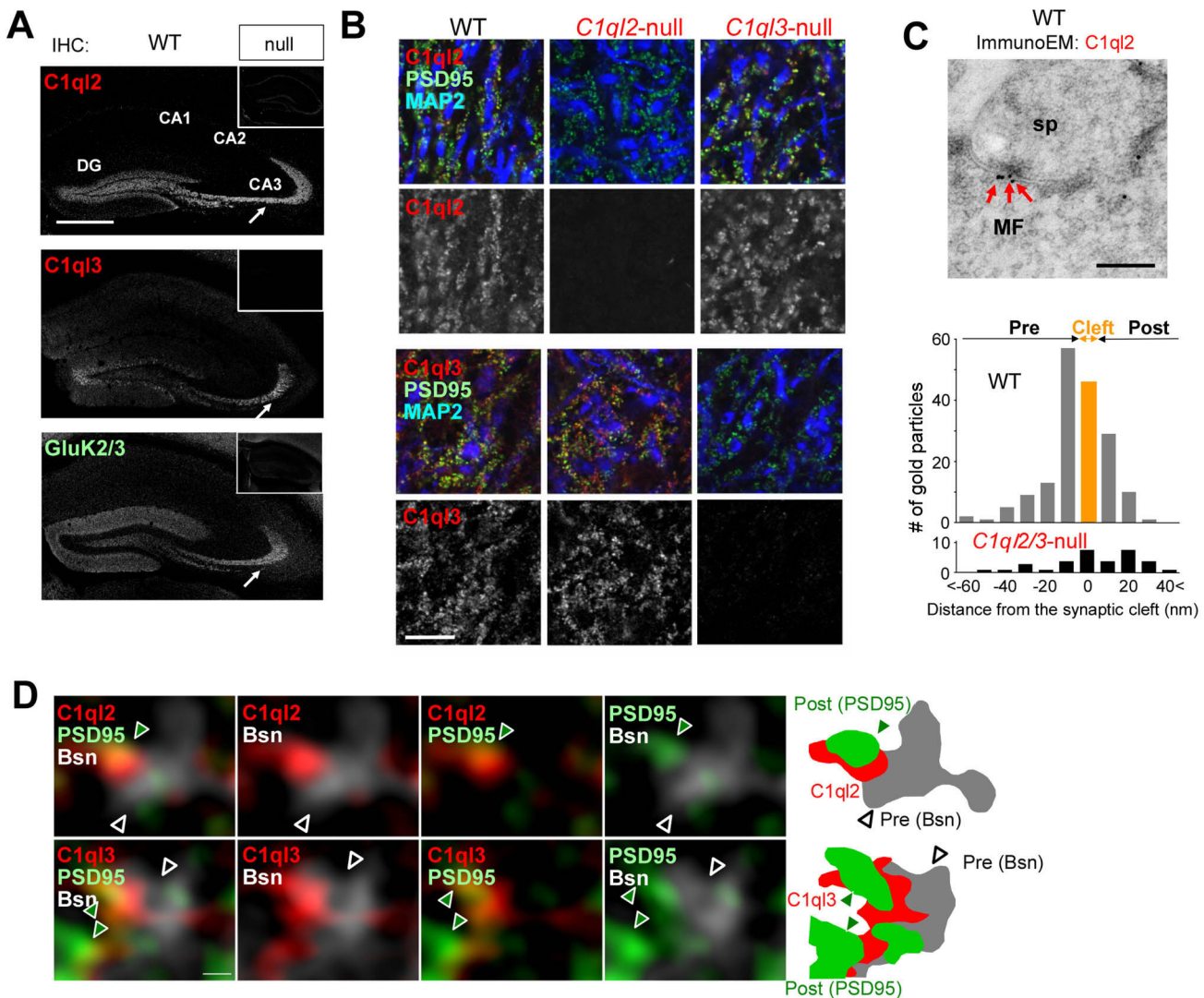


**Figure 1. C1ql2 and C1ql3 are Localized at MF-CA3 Synapses**

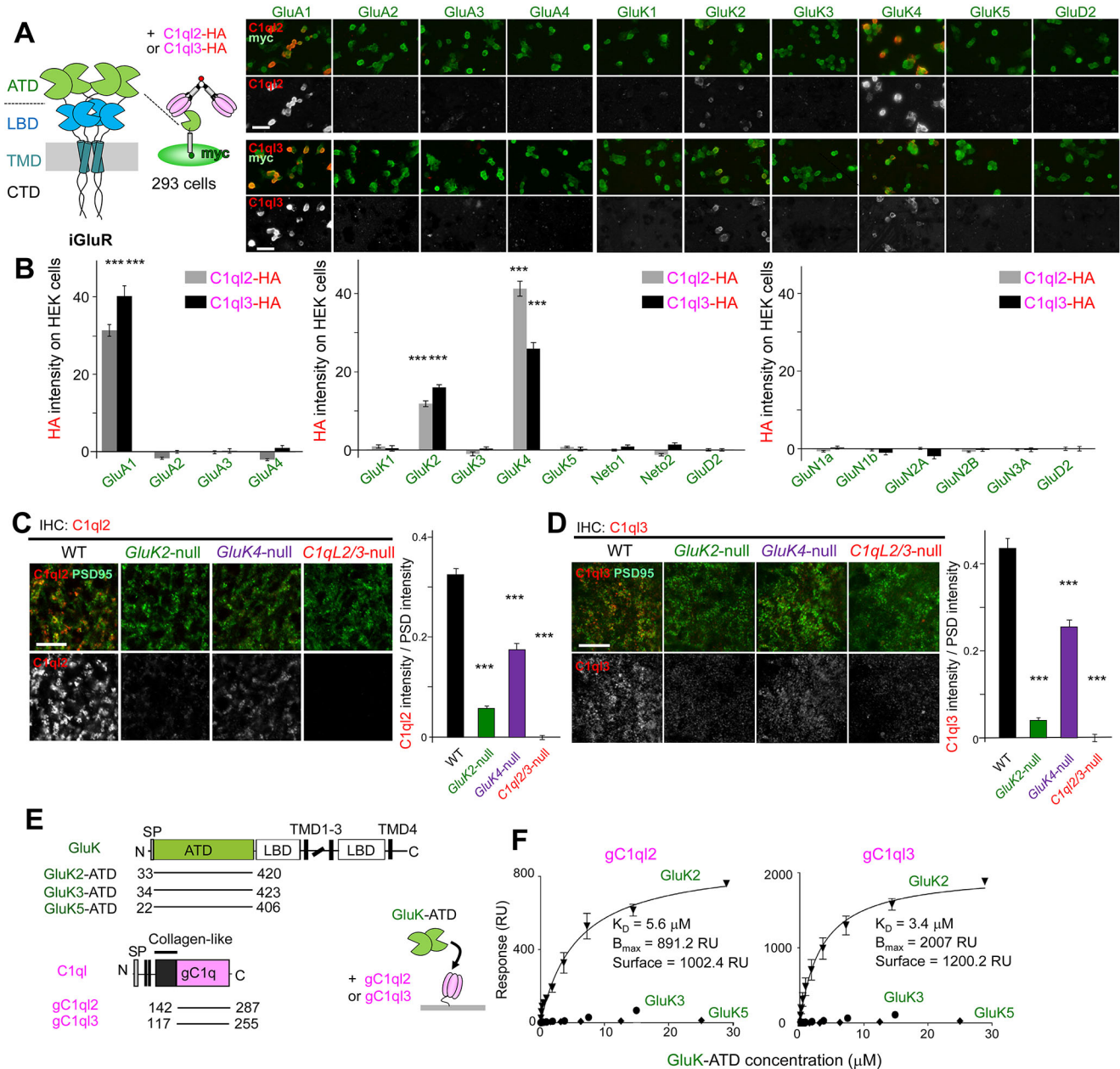


**Figure. 2. Direct Interaction between C1q2/3 and ATDs of iGluRs**

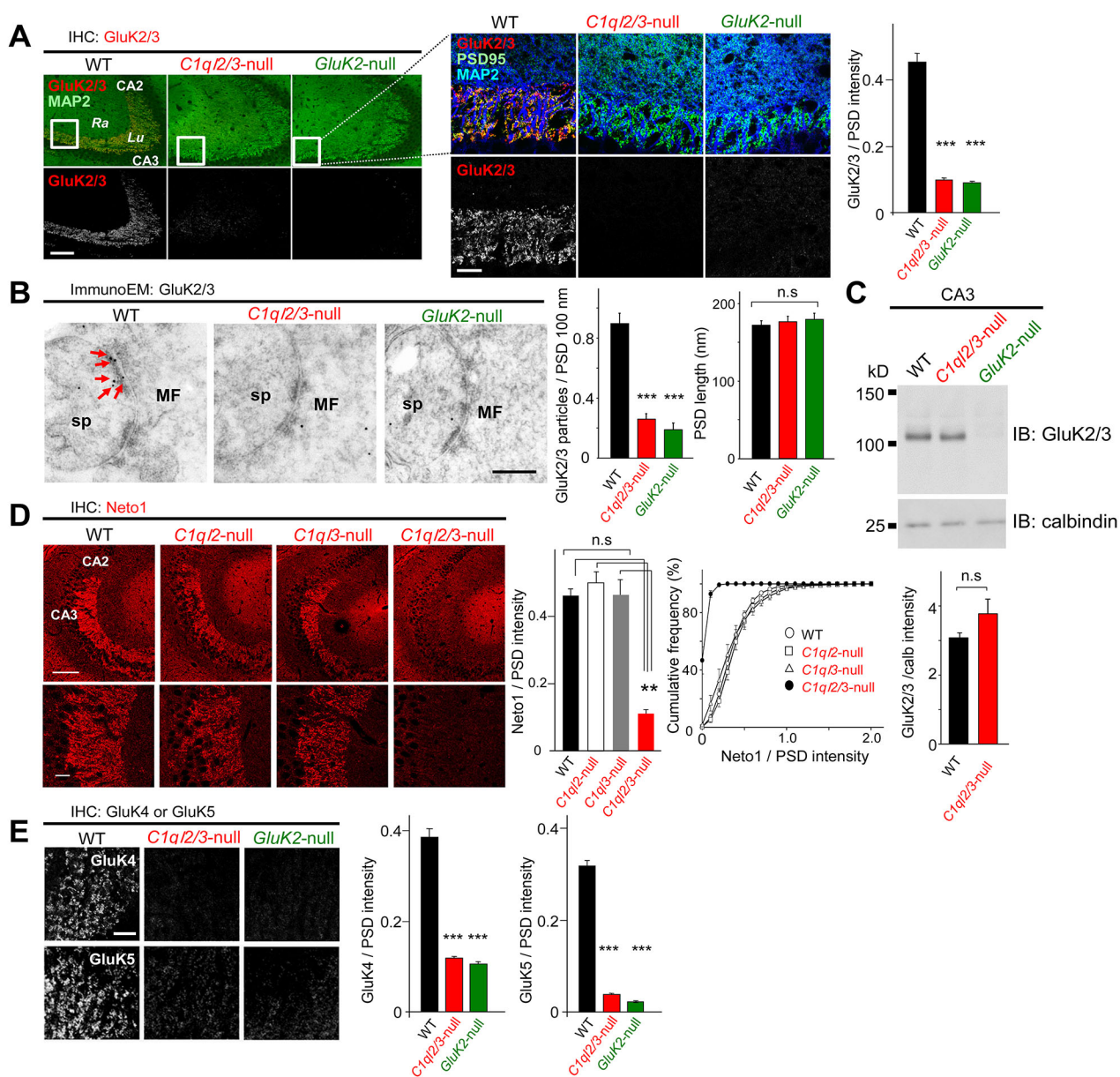
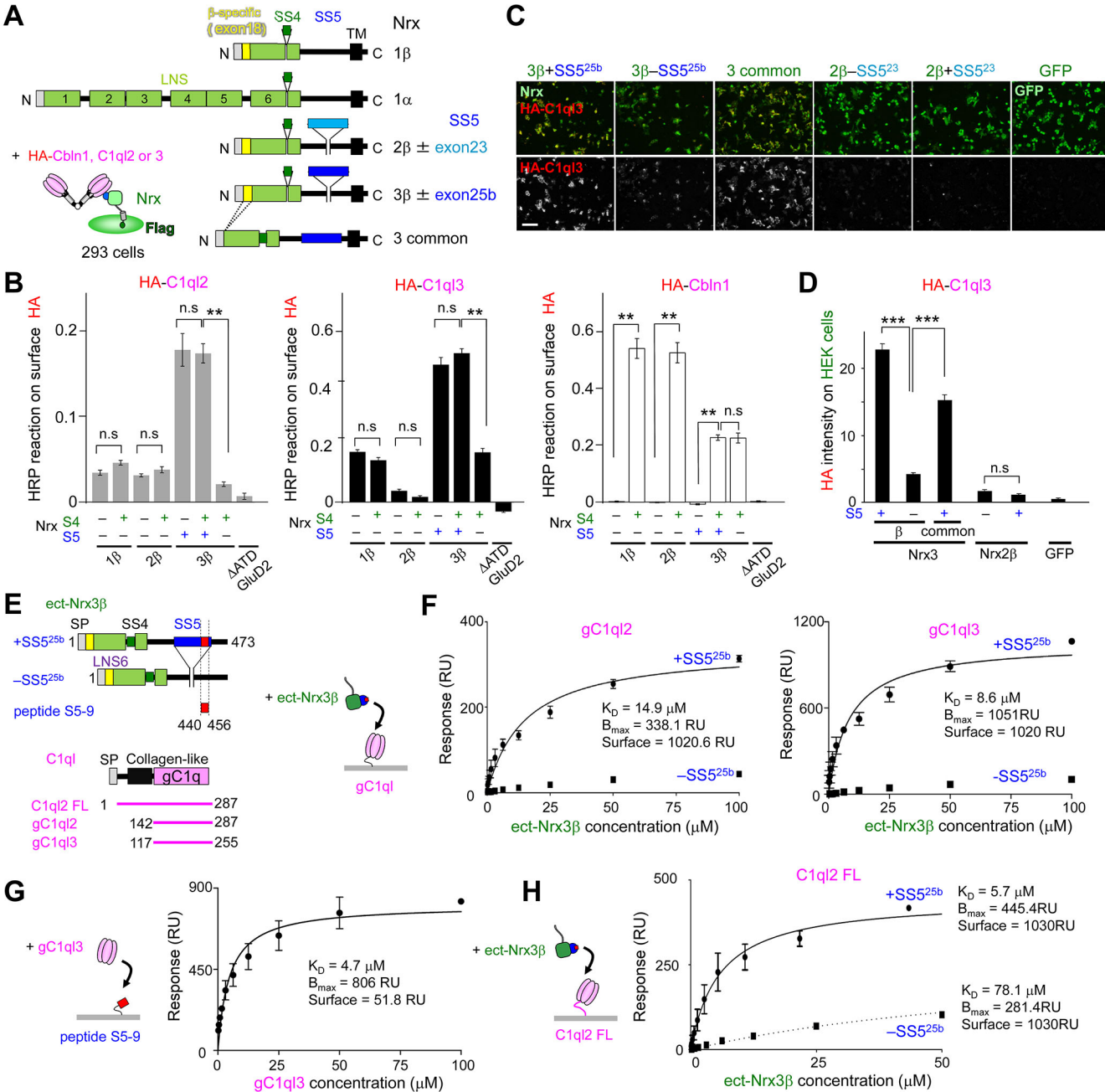


Figure 3. C1q2 and C1q3 Determine Postsynaptic KAR Localization at MF-CA3 Synapses



**Figure 4. Direct Interaction between C1ql2/3 and Nr3+SS5<sup>25b</sup>**

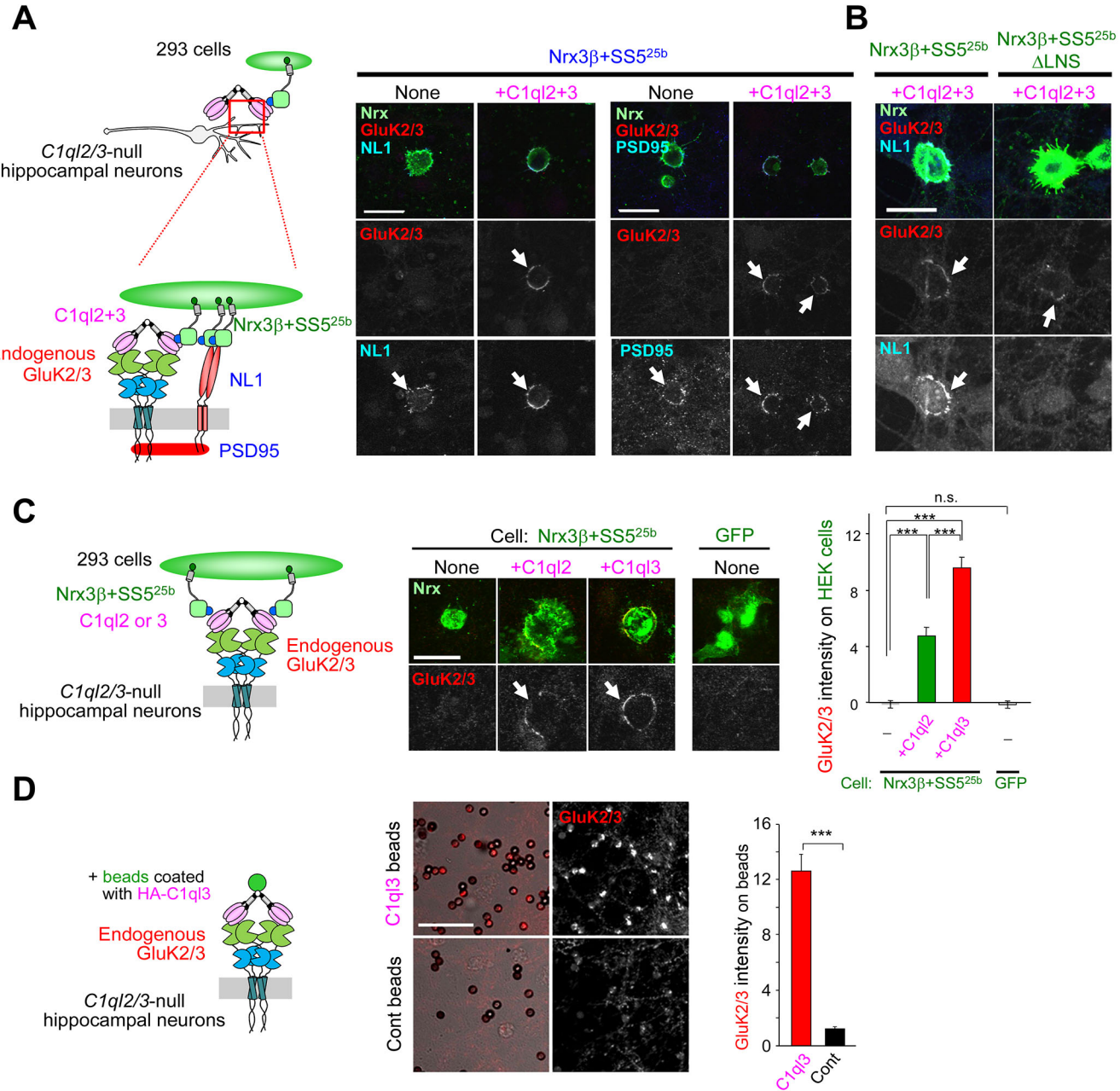
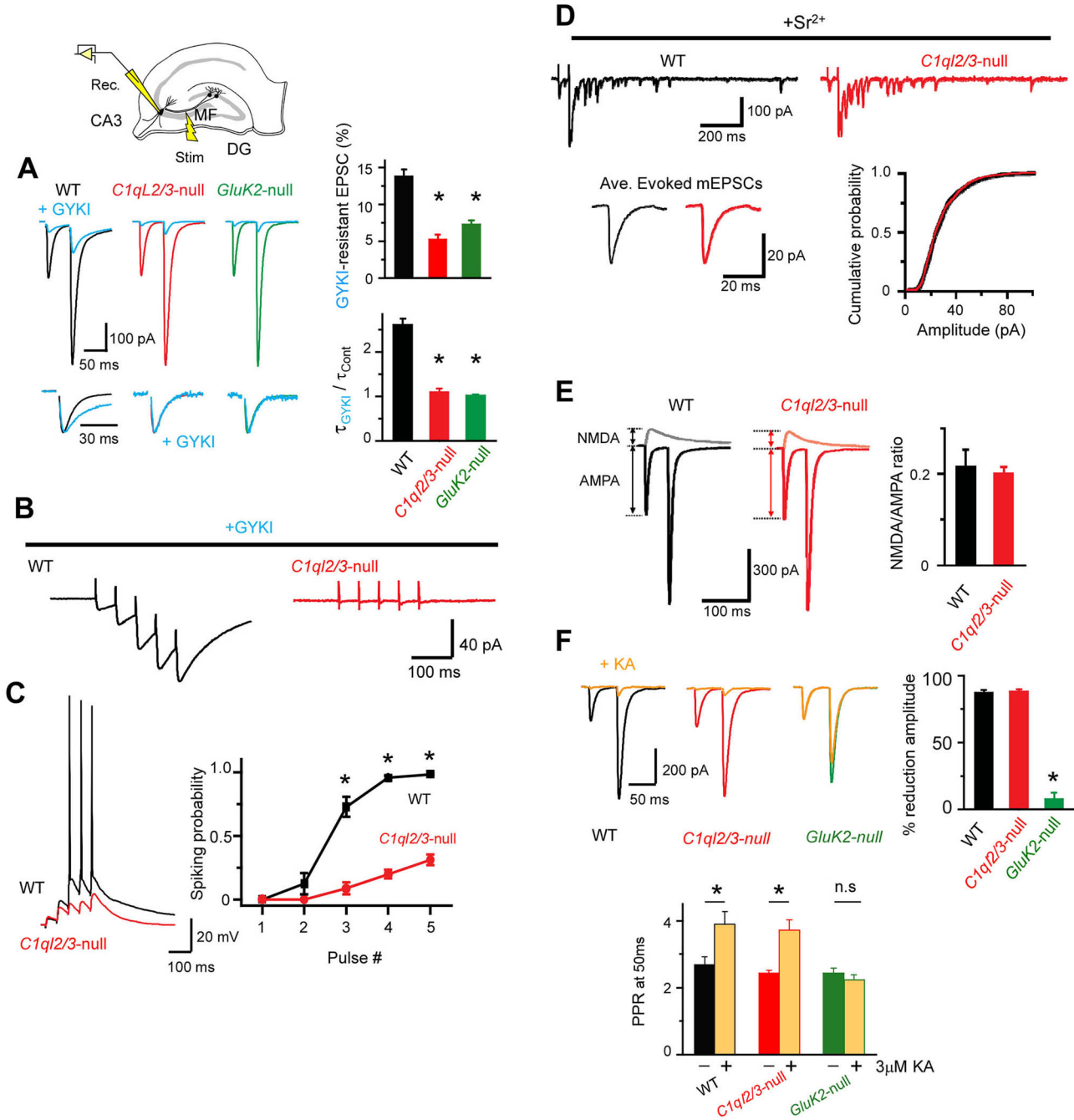
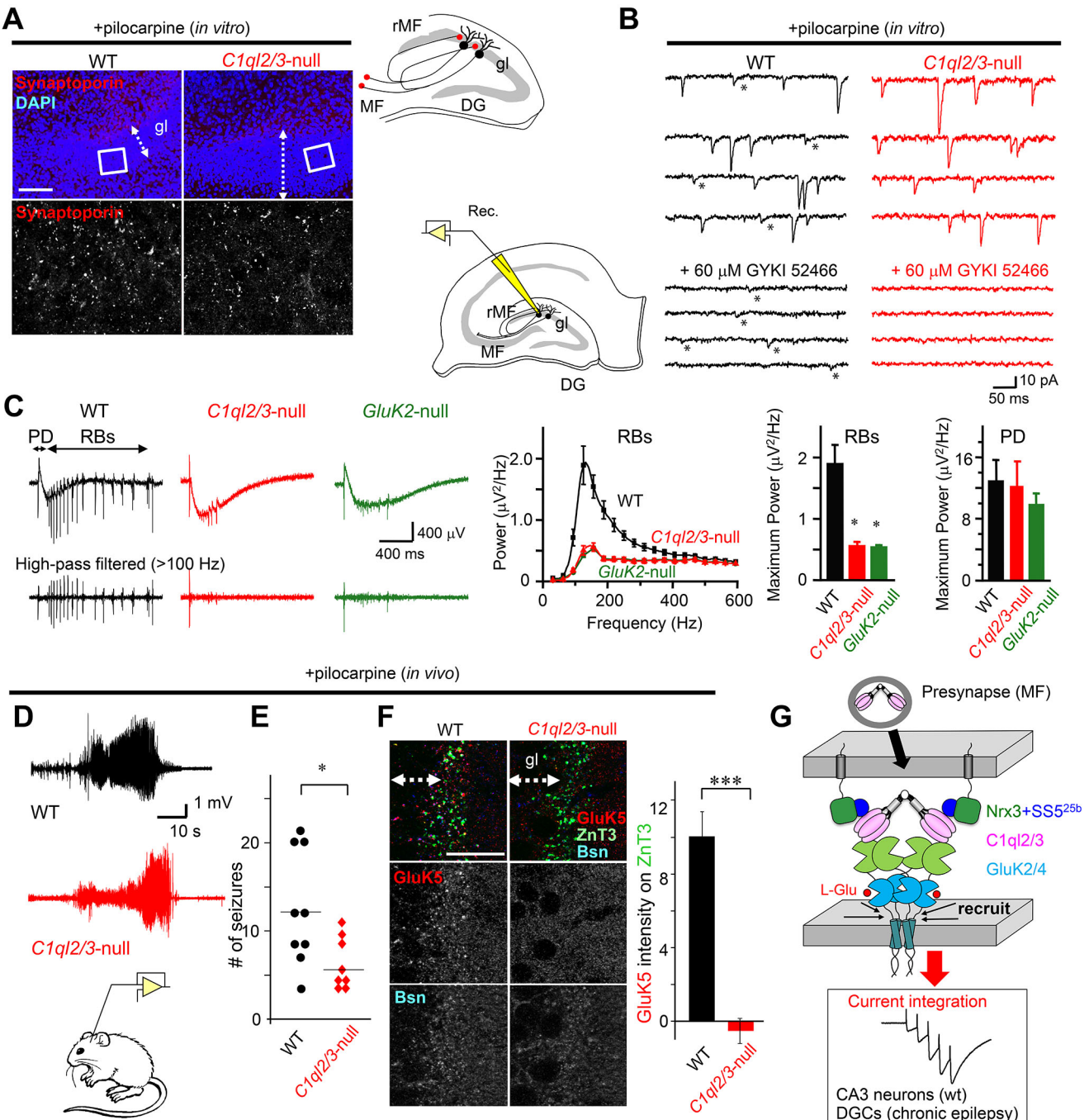


Figure 5. Nrx3–C1q/2/3 Signaling Recruits KARs in Cultured Hippocampal Neurons



**Figure 6. C1ql2/3 Determine Postsynaptic KAR Functions in the Hippocampus**



**Figure 7. C1ql2/3 Regulate Postsynaptic Localization of KARs in Sprouted MFs and Contribute to Recurrent Circuit Activities in Chronic Epilepsy Models**